Journal of Molecular Structure xxx (xxxx) xxx

Contents lists available at ScienceDirect

Journal of Molecular Structure

journal homepage: www.elsevier.com/locate/molstr

An extensive research on aldose reductase inhibitory effects of new 4*H*-1,2,4-triazole derivatives

Belgin Sever[a,*], Mehlika Dilek Altıntop[a], Yeliz Demir[b], Muhammed Pekdoğan[a], Gülşen Akalın Çiftçi[c], Şükrü Beydemir[c,d], Ahmet Özdemir[a]

[a] Department of Pharmaceutical Chemistry, Faculty of Pharmacy, Anadolu University, 26470, Eskişehir, Turkey
[b] Department of Pharmacy Services, Nihat Delibalta Gole Vocational High School, Ardahan University, 75700, Ardahan, Turkey
[c] Department of Biochemistry, Faculty of Pharmacy, Anadolu University, 26470, Eskişehir, Turkey
[d] The Rectorate of Bilecik Şeyh Edebali University, 11230, Bilecik, Turkey

ARTICLE INFO

Article history:
Received 8 September 2020
Revised 2 October 2020
Accepted 12 October 2020
Available online xxx

Keywords:
Triazole
Thiazole
Benzothiazole
Aldose reductase
Diabetic complications
Cytotoxicity
Molecular docking

ABSTRACT

Aldose reductase (AR) is a key enzyme, which triggers the excessive accumulation of sorbitol in insulin independent tissues leading to severe diabetes-induced microvascular complications. Substantial evidence has proven that AR inhibition is a well-established strategy to attenuate these complications. In the current work, new 2-[(4-amino-5-aryl-4*H*-1,2,4-triazol-3-yl)thio]-*N*-(thiazol/benzothiazol-2-yl)acetamides (**1**–**18**) were synthesized and evaluated for their inhibitory capacities on AR. 2-[(4-Amino-5-(4-methylphenyl)-4*H*-1,2,4-triazol-3-yl)thio]-*N*-(5-nitrothiazol-2-yl)acetamide (**12**) and 2-[(4-amino-5-(3-pyridyl)-4*H*-1,2,4-triazol-3-yl)thio]-*N*-(6-nitrobenzothiazol-2-yl)acetamide (**17**) were identified as the most effective AR inhibitors in this series with the K_i values of 0.04 ± 0.01 μM and 0.08 ± 0.02 μM, respectively as compared to quercetin (K_i = 5.66 ± 0.66 μM). These two compounds displayed competitive AR inhibition. MTT assay, a tetrazolium-based cell viability assay, was performed to determine the cytotoxic effects of compounds **1**–**18** on L929 mouse fibroblast (healthy) cell line. Compounds **1**–**18**, except for compounds **10, 13, 14, 15** and **16**, were found nontoxic against healthy cells. Besides, molecular docking studies were fundamentally in agreement with the biological data with regard to essential π-π interactions with Trp219, Phe122 and Trp111 residues in the active site of AR. Eventually, *in vitro* and *in silico* assays ascertain that in particular compounds **12** and **17** will attract a great notice as drug-like AR inhibitors for further investigations related to amelioration of long-term diabetic complications.

1. Introduction

Diabetes Mellitus (DM) is a chronic and multi-factorial disease characterised by impaired glucose homeostasis due to abnormal insulin action [1–3]. Among two major forms of DM, type 1 or insulin dependent DM (T1DM) is the result of immune mediated genetically programmed devastation of the β-cells, whereas type 2 or non-insulin dependent DM (T2DM) stems from the insufficient insulin secretion and/or the insulin resistance [4,5].

It is well known that patients with DM show a tendency to develop one or more of the secondary diabetic complications including cataract, retinopathy, nephropathy and neuropathy in the course of their disease [6,7]. These long-term microvascular complications are also associated with the formation of blindness, end stage renal failure, defective nerve conduction and impaired wound healing [8]. There are several mechanisms implicated in the progression of these microvascular disorders such as elevated activity of polyol and hexosamine pathways, excessive advanced glycation end products (AGEs) and protein kinase C (PKC) isoforms and inadequate antioxidant defense [9,10].

Polyol pathway is normally an alternative route for glucose metabolism, whereas in hyperglycemia, there is a marked rise in flux through this pathway detrimentally affecting tissues such as retina, kidney, peripheral nerves and blood vessels where glucose entry is independent of insulin [11,12]. Aldose reductase (AR) drives the nicotinamide adenine dinucleotide phosphate (reduced form) (NADPH)-dependent conversion of glucose to sorbitol as a first and rate limiting enzyme in the polyol pathway (Fig. 1). Sorbitol, in turn is oxidized to fructose by nicotinamide adenine dinucleotide $(NAD)^+$-dependent sorbitol dehydrogenase (SDH) [13]. Augmented AR levels along with the depletion of NADPH have been reported to lead to oxidative stress and the accumulation of intracellular sorbitol along with the increased free NADH/NAD^+

* Corresponding author.
E-mail address: belginsever@anadolu.edu.tr (B. Sever).

https://doi.org/10.1016/j.molstruc.2020.129446
0022-2860/

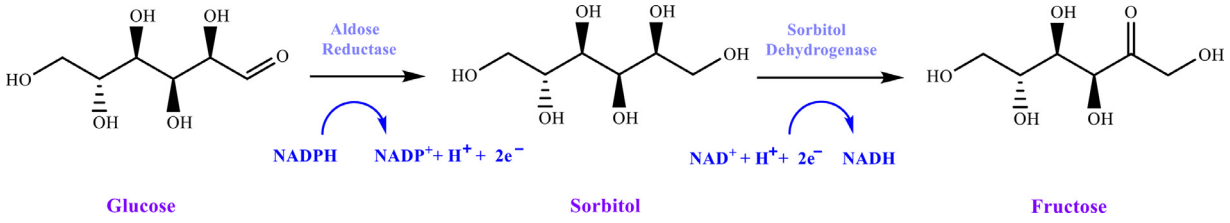

Fig. 1. The polyol pathway.

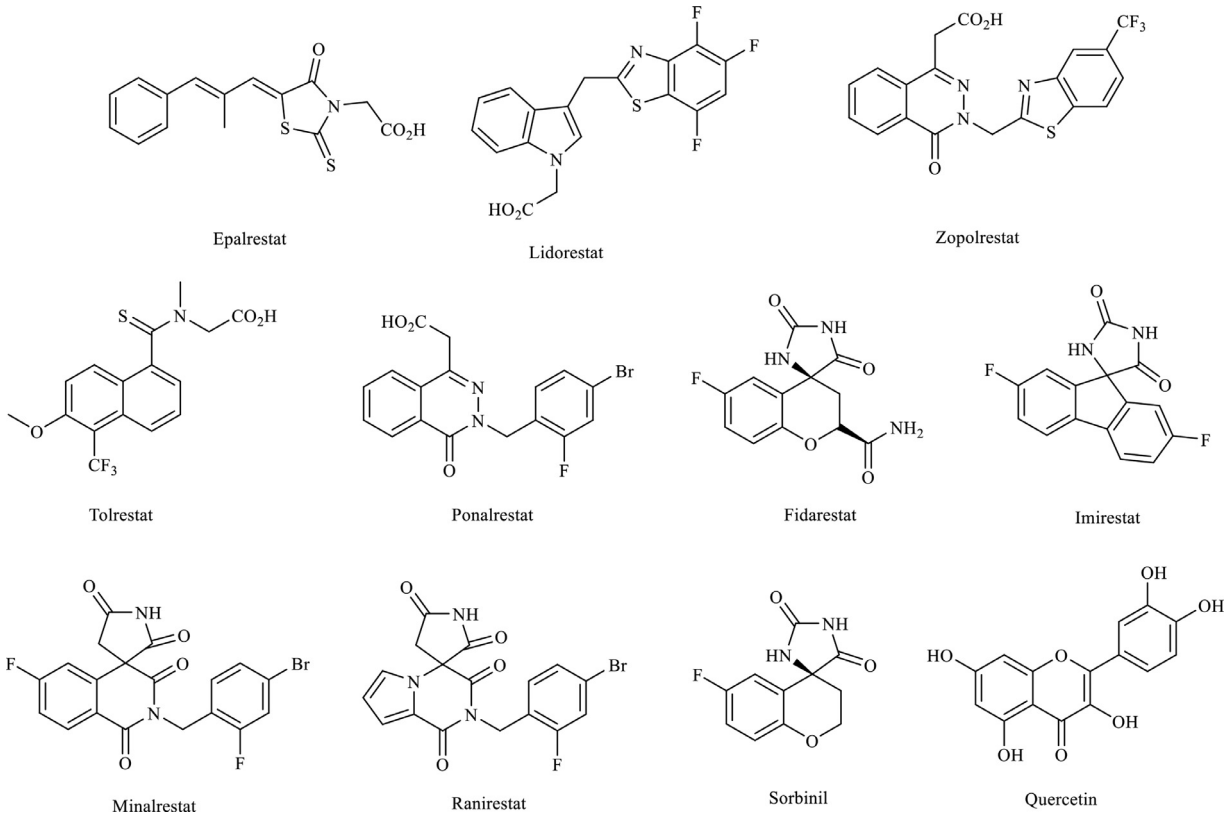

Fig. 2. Some AR inhibitors.

ratio, which triggers osmotic stress [14–16]. Based upon substantial experimental data linking the AR inhibition with the alleviation of secondary diabetic lesions, research efforts have focused on understanding the structure and function of AR and developing effective anti-AR interventions [17,18].

On the basis of safety and efficacy issues and poor pharmacokinetic profiles, the development of many AR inhibitors (Fig. 2) was terminated. Epalrestat, which was launched into Japanese market in 1992, is the only currently commercially available AR inhibitor. Sorbinil has been reported to show *in vitro* and *in vivo* AR inhibitory activity after comprehensive tests, but it was pulled from the market owing to emerging hypersensitivity reactions. Besides, among flavonoids quercetin exhibited dual AR inhibitory and antioxidant effects, whereas its oral bioavailability was found quite low due to its high hydrophilicity [19–22]. In order to design and synthesize new potent AR inhibitors, some physicochemical parameters related to crossing biological membranes easily and selectivity due to the coexistence of AR with aldehyde reductase in most tissues must be enlightened [19].

Triazole is a five-membered heterocyclic pharmacophore system bearing three nitrogen and two carbon atoms. 1,2,3-Triazole and 1,2,4-triazole are two isomeric forms of triazole. Triazoles have been reported to possess assorted pharmacological activites including antidiabetic activity based on its moderate dipole character, π-π stacking interactions and hydrogen bonding capability, rigidity, improved solubility and stability to metabolic degradation and redox conditions. These properties of triazole scaffold also play important roles in high-affinity binding with the biological targets [23–33]. On the other hand, compounds carrying a benzothiazole ring just as in zopolrestat have been enunciated to present higher selectivity for AR fitting into the hydrophobic pocket. It is also well ascertained that some thiazole derivatives show very potent AR inhibition [34–37].

Such challenging observations mentioned above have prompted us to synthesize new 4*H*-1,2,4-triazole derivatives clubbed with thiazole/benzothiazole scaffolds (**1**–**18**), to investigate their AR inhibitory effects, to evaluate their cytotoxicity against L929 mouse fibroblast (healthy) cells and to *in silico* explore their possible binding modes in the active site of AR along with their pharmacokinetic profiles.

2. Experimental

2.1. Chemistry

All reagents purchased from commercial suppliers were used without additional purification. The Electrothermal IA9200 digital melting point apparatus (Staffordshire, UK) was used for the deter-

mination of the melting points (M.p.) of the compounds. IR spectra were recorded on an IRPrestige-21 Fourier Transform Infrared spectrophotometer (Shimadzu, Tokyo, Japan). ^{1}H NMR and ^{13}C NMR spectra were recorded on a Bruker 400 MHz spectrometer (Bruker, Billerica, MA, USA) using DMSO–d_6 as a solvent. Chemical shifts were reported in parts per million (ppm). Tetramethylsilane (TMS) was used as an internal standard. In the NMR spectra, the splitting patterns were designated as follows: s: singlet; d: doublet; t: triplet; m: multiplet. Coupling constants (*J*) were reported in Hertz (Hz). HRMS spectra were recorded on a Shimadzu LCMS-IT-TOF system (Shimadzu, Kyoto, Japan) using methanol as a solvent. Thin Layer Chromatography (TLC) was performed on TLC Silica gel 60 F_{254} aluminum sheets (Merck, Darmstadt, Germany) to control the purity of the compounds.

2.1.1. General procedure for the synthesis of the compounds

*2.1.1.1. 4-Amino-5-aryl-4H-1,2,4-triazole-3-thiol (**A**).* A mixture of 5-aryl-1,3,4-oxadiazole-2-thiol (0.01 mol) and hydrazine hydrate (0.01 mol) in absolute ethanol was refluxed for 12 h. Then, the solvent was removed under reduced pressure. 100 mL of cold water was added to residue and later, acidified with concentrated HCl to pH = 5. Finally, the obtained product was filtered off and crystallized from ethanol [38].

2.1.1.2. 2-Chloro-N-(aryl)acetamides. Chloroacetyl chloride (0.03 mol) was added dropwise to a mixture of aromatic amine (0.025 mol) and triethylamine (TEA) (0.025 mol) in toluene (50 mL) at 0–5 °C. The solvent was evaporated under reduced pressure. The residue was washed with water to remove TEA and crystallized from ethanol. The products were crystallized from ethanol [39].

*2.1.1.3. 2-[(4-*Amino-*5-*aryl-*4H-1,2,4-*triazol-*3-*yl*)*thio*]-N-(thiazol/benzothiazol-2-yl)acetamides (**1**–**18**).* A mixture of compound **A** (0.0015 mol) and appropriate 2–chloro–*N*-(aryl)acetamide (0.0015 mol) in acetone (25 mL) was stirred at room temperature for 8 h in the presence of potassium carbonate (0.0015 mol). The solvent was evaporated under reduced pressure. The residue was washed with water and crystallized from ethanol [40].

*2.1.1.3.1. 2-[(4-*Amino-*5-(4-*methoxyphenyl*)–4H-1,2,4-*triazol-3-*yl*)*thio*]-N-(benzothiazol-2-yl)acetamide (**1**).* M.p.: 208–209 °C. Yield: 80%. IR ν_{max} (cm^{-1}): 3350, 3280 (N–H stretching), 3176, 3062 (Aromatic C–H stretching), 2972, 2935, 2839 (Aliphatic C–H stretching), 1680 (Amide C=O stretching), 1602, 1564, 1556, 1471 (N–H bending, C=N and C=C stretching), 1436, 1392, 1336, 1294, 1253, 1178, 1097, 1026 (C–H bending, C–N and C–O stretching, aromatic C–H in plane bending), 970, 893, 873, 833, 800, 752, 729, 694 (Aromatic C–H out of plane bending and C-S stretching) (Supplementary Material Fig. S1). ^{1}H NMR (400 MHz, DMSO–d_6): 3.81 (s, 3H), 4.15 (s, 2H), 6.32 (s, 2H), 7.06 (d, *J* = 8.40 Hz, 2H), 7.18 (t, *J* = 7.20, 7.60, 14.80 Hz, 1H), 7.34 (t, *J* = 7.20, 7.60, 14.80 Hz, 1H), 7.64 (d, *J* = 7.60 Hz, 1H), 7.83 (d, *J* = 7.60 Hz, 1H), 7.97 (d, *J* = 8.80 Hz, 2H), 12.56 (s, 1H) (Supplementary Material Fig. S2). ^{13}C NMR (100 MHz, DMSO–d_6): 37.4 (CH_2), 55.3 (CH_3), 113.9 (2CH), 119.3 (CH), 119.8 (CH), 121.3 (C), 122.3 (CH), 125.4 (CH), 129.3 (2CH), 132.0 (C), 149.3 (C), 152.9 (C), 153.9 (C), 160.3 (C), 162.2 (C), 169.7 (C) (Supplementary Material Fig. S3). HRMS (ESI) (*m/z*) $[M + H]^+$ calcd. for $C_{18}H_{16}N_6O_2S_2$: 413.0849, found: 413.0858 (Supplementary Material Fig. S4).

*2.1.1.3.2. 2-[(4-*Amino-*5-(4-*methoxyphenyl*)–4H-1,2,4-*triazol-3-*yl*)*thio*]-N-(6-chlorobenzothiazol-2-yl)acetamide (**2**).* M.p.: 248–249 °C. Yield: 79%. IR ν_{max} (cm^{-1}): 3381, 3338 (N–H stretching), 3118, 3062, 3005 (Aromatic C–H stretching), 2964, 2920, 2835 (Aliphatic C–H stretching), 1664 (Amide C=O stretching), 1600, 1558, 1479, 1462 (N–H bending, C=N and C=C stretching), 1442, 1388, 1327, 1305, 1251, 1174, 1099, 1037 (C–H bending, C–N and C–O stretching, aromatic C–H in plane bending), 966, 883, 825, 802, 765, 738, 688 (Aromatic C–H out of plane bending and C-S stretching) (Supplementary Material Fig. S5). ^{1}H NMR (400 MHz, DMSO–d_6): 3.77 (s, 3H), 4.25 (s, 2H), 6.16 (s, 2H), 7.03 (s, 3H), 7.41 (s, 2H), 7.71–8.07 (m, 2H), 12.74 (s, 1H) (Supplementary Material Fig. S6). ^{13}C NMR (100 MHz, DMSO–d_6): 34.8 (CH_2), 55.2 (CH_3), 113.9 (2CH), 119.0 (CH), 121.3 (CH), 121.7 (C), 126.4 (CH), 127.5 (C), 129.0 (CH), 129.1 (CH), 133.1 (C), 147.4 (C), 152.5 (C), 154.0 (C), 158.9 (C), 160.2 (C), 167.9 (C) (Supplementary Material Fig. S7). HRMS (ESI) (*m/z*) $[M + H]^+$ calcd. for $C_{18}H_{15}ClN_6O_2S_2$: 447.0459, found: 447.0460 (Supplementary Material Fig. S8).

*2.1.1.3.3. 2-[(4-*Amino-*5-(4-*methoxyphenyl*)–4H-1,2,4-*triazol-3-*yl*)*thio*]-N-(6-bromobenzothiazol-2-yl)acetamide (**3**).* M.p.: 243–244 °C. Yield: 84%. IR ν_{max} (cm^{-1}): 3379, 3336 (N–H stretching), 3149, 3115, 3061 (Aromatic C–H stretching), 2999, 2960, 2920, 2833 (Aliphatic C–H stretching), 1664 (Amide C=O stretching), 1595, 1556, 1539, 1479, 1462 (N–H bending, C=N and C=C stretching), 1440, 1388, 1323, 1305, 1251, 1226, 1174, 1111, 1085, 1037 (C–H bending, C–N and C–O stretching, aromatic C–H in plane bending), 964, 869, 825, 802, 731 (Aromatic C–H out of plane bending and C-S stretching) (Supplementary Material Fig. S9). ^{1}H NMR (400 MHz, DMSO–d_6): 3.81 (s, 3H), 4.29 (s, 2H), 6.21 (s, 2H), 7.06 (d, *J* = 9.20 Hz, 2H), 7.56 (d, *J* = 8.80 Hz, 1H), 7.69 (d, *J* = 8.80 Hz, 1H), 7.93 (d, *J* = 9.20 Hz, 2H), 8.23 (s, 1H), 12.72 (s, 1H) (Supplementary Material Fig. S10). ^{13}C NMR (100 MHz, DMSO–d_6): 34.9 (CH_2), 55.2 (CH_3), 113.9 (2CH), 115.4 (C), 119.1 (CH), 122.1 (CH), 124.2 (C), 129.1 (CH), 129.2 (2CH), 133.7 (C), 147.7 (C), 152.5 (C), 154.0 (C), 159.0 (C), 160.3 (C), 168.0 (C) (Supplementary Material Fig. S11). HRMS (ESI) (*m/z*) $[M + H]^+$ calcd. for $C_{18}H_{15}BrN_6O_2S_2$: 490.9954, found: 490.9967 (Supplementary Material Fig. S12).

*2.1.1.3.4. 2-[(4-*Amino-*5-(4-*methoxyphenyl*)–4H-1,2,4-*triazol-3-*yl*)*thio*]-N-(6-methylbenzothiazol-2-yl)acetamide (**4**).* M.p.: 252–253 °C. Yield: 92%. IR ν_{max} (cm^{-1}): 3342, 3265 (N–H stretching), 3199, 3003 (Aromatic C–H stretching), 2968, 2931, 2837 (Aliphatic C–H stretching), 1687 (Amide C=O stretching), 1614, 1554, 1481, 1456 (N–H bending, C=N and C=C stretching), 1415, 1390, 1307, 1282, 1259, 1226, 1168, 1099, 1037 (C–H bending, C–N and C–O stretching, aromatic C–H in plane bending), 997, 968, 893, 813, 744, 713, 680 (Aromatic C–H out of plane bending and C-S stretching) (Supplementary Material Fig. S13). ^{1}H NMR (400 MHz, DMSO–d_6): 2.34 (s, 3H), 3.81 (s, 3H), 3.90 (s, 2H), 6.45 (s, 2H), 7.01–7.10 (m, 3H), 7.36 (d, *J* = 7.60 Hz, 1H), 7.46 (s, 1H), 7.99 (d, *J* = 8.40 Hz, 2H), 12.65 (s, 1H) (Supplementary Material Fig. S14). ^{13}C NMR (100 MHz, DMSO–d_6): 20.9 (CH_3), 40.6 (CH_2), 55.2 (CH_3), 113.8 (2CH), 118.4 (CH), 119.6 (CH), 120.5 (C), 125.6 (CH), 129.3 (2CH), 129.6 (C), 132.9 (C), 148.1 (C), 153.1 (C), 153.5 (C), 160.1 (C), 166.7 (C), 171.6 (C) (Supplementary Material Fig. S15). HRMS (ESI) (*m/z*) $[M + H]^+$ calcd. for $C_{19}H_{18}N_6O_2S_2$: 427.1005, found: 427.1006 (Supplementary Material Fig. S16).

*2.1.1.3.5. 2-[(4-*Amino-*5-(4-*methoxyphenyl*)–4H-1,2,4-*triazol-3-*yl*)*thio*]-N-(6-nitrobenzothiazol-2-yl)acetamide (**5**).* M.p.: 212–213 °C. Yield: 86%. IR ν_{max} (cm^{-1}): 3332, 3211 (N–H stretching), 3091 (Aromatic C–H stretching), 2972, 2927, 2839 (Aliphatic C–H stretching), 1693 (Amide C=O stretching), 1610, 1575, 1552, 1504, 1460 (N–H bending, NO_2, C=N and C=C stretching), 1435, 1323, 1286, 1255, 1226, 1168, 1124, 1045, 1028 (C–H bending, C–N and C–O stretching, aromatic C–H in plane bending), 975, 881, 825, 800, 750, 732 (Aromatic C–H out of plane bending and C-S stretching) (Supplementary Material Fig. S17). ^{1}H NMR (400 MHz, DMSO–d_6): 3.81 (s, 3H), 4.11 (s, 2H), 6.31 (s, 2H), 7.06 (d, *J* = 8.40 Hz, 2H), 7.64 (d, *J* = 9.20 Hz, 1H), 7.96 (d, *J* = 8.40 Hz, 2H), 8.14 (d, *J* = 8.40 Hz, 1H), 8.74 (s, 1H), 12.71 (s, 1H) (Supplementary Material Fig. S18). ^{13}C NMR (100 MHz, DMSO–d_6): 36.6 (CH_2), 55.2 (CH_3), 113.8 (2CH), 117.8 (CH), 118.6 (CH), 119.4 (C), 121.0 (CH), 129.3 (2CH), 132.8 (C), 141.1 (C), 152.9 (C), 153.7 (C),

155.7 (C), 160.2 (C), 170.4 (C), 172.6 (C) (Supplementary Material Fig. S19). HRMS (ESI) (*m/z*) $[M + H]^+$ calcd. for $C_{18}H_{15}N_7O_4S_2$: 458.0700, found: 458.0677 (Supplementary Material Fig. S20).

*2.1.1.3.6. 2-[(4-*Amino*-5-(4-*methoxyphenyl*)−4H-1,2,4-*triazol*-3-*yl*)thio*]*-N-(5-nitrothiazol-2-yl)acetamide (**6**).* M.p.: 184–185 °C. Yield: 55%. IR ν_{max} (cm^{-1}): 3352, 3307 (N–H stretching), 3149, 3093, 3008 (Aromatic C–H stretching), 2929, 2835 (Aliphatic C–H stretching), 1672 (Amide C=O stretching), 1610, 1575, 1504, 1481, 1460 (N–H bending, NO_2, C=N and C=C stretching), 1417, 1381, 1286, 1253, 1172, 1122, 1029 (C–H bending, C–N and C–O stretching, aromatic C–H in plane bending), 962, 935, 904, 827, 732, 678, 646 (Aromatic C–H out of plane bending and C-S stretching) (Supplementary Material Fig. S21). ^{1}H NMR (400 MHz, DMSO–d_6): 3.81 (s, 3H), 4.06 (s, 2H), 5.77 and 6.28 (2s, 2H), 7.05–7.09 (m, 2H), 7.95–8.00 (m, 2H), 8.48 (s, 1H), 12.75 (s, 1H) (Supplementary Material Fig. S22). ^{13}C NMR (100 MHz, DMSO–d_6): 39.4 (CH_2), 55.3 (CH_3), 113.9 (CH), 113.9 (CH), 119.4 (C), 129.3 (CH), 129.6 (CH), 137.0 (C), 145.6 (CH), 152.8 (C), 153.7 (C), 160.2 (C), 166.5 (C), 172.0 (C) (Supplementary Material Fig. S23). HRMS (ESI) (*m/z*) $[M + H]^+$ calcd. for $C_{14}H_{13}N_7O_4S_2$: 408.0543, found: 408.0538 (Supplementary Material Fig. S24).

*2.1.1.3.7. 2-[(4-*Amino*-5-(4-*methylphenyl*)−4H-1,2,4-*triazol*-3-*yl*)thio*]*-N-(benzothiazol-2-yl)acetamide (**7**).* M.p.: 204–205 °C. Yield: 75%. IR ν_{max} (cm^{-1}): 3338, 3275 (N–H stretching), 3176, 3059 (Aromatic C–H stretching), 2918, 2841 (Aliphatic C–H stretching), 1668 (Amide C=O stretching), 1614, 1556, 1485, 1460 (N–H bending, C=N and C=C stretching), 1438, 1381, 1321, 1282, 1265, 1224, 1172, 1126, 1028 (C–H bending, C–N and C–O stretching, aromatic C–H in plane bending), 975, 943, 879, 821, 750, 721, 680 (Aromatic C–H out of plane bending and C-S stretching) (Supplementary Material Fig. S25). ^{1}H NMR (400 MHz, DMSO–d_6): 2.36 (s, 3H), 4.23 (s, 2H), 6.28 (s, 2H), 7.20–7.47 (m, 4H), 7.70 (d, J = 8.40 Hz, 1H), 7.89 (d, J = 7.60 Hz, 3H), 12.78 (s, 1H) (Supplementary Material Fig. S26). ^{13}C NMR (100 MHz, DMSO–d_6): 20.9 (CH_3), 36.1 (CH_2), 120.1 (CH), 121.4 (CH), 122.9 (CH), 124.0 (CH), 127.4 (C), 127.6 (2CH), 129.0 (2CH), 131.7 (C), 139.3 (C), 148.9 (C), 153.0 (C), 154.1 (C), 160.1 (C), 168.6 (C) (Supplementary Material Fig. S27). HRMS (ESI) (*m/z*) $[M + H]^+$ calcd. for $C_{18}H_{16}N_6OS_2$: 397.0900, found: 397.0904 (Supplementary Material Fig. S28).

*2.1.1.3.8. 2-[(4-*Amino*-5-(4-*methylphenyl*)−4H-1,2,4-*triazol*-3-*yl*)thio*]*-N-(6-chlorobenzothiazol-2-yl)acetamide (**8**).* M.p.: 258–259 °C. Yield: 83%. IR ν_{max} (cm^{-1}): 3329, 3250 (N–H stretching), 3182 (Aromatic C–H stretching), 2981, 2922, 2856 (Aliphatic C–H stretching), 1681 (Amide C=O stretching), 1622, 1591, 1550, 1483 (N–H bending, C=N and C=C stretching), 1442, 1423, 1404, 1323, 1280, 1238, 1178, 1130, 1103, 1043 (C–H bending, C–N and C–O stretching, aromatic C–H in plane bending), 975, 941, 894, 858, 827, 806, 744 (Aromatic C–H out of plane bending and C-S stretching) (Supplementary Material Fig. S29). ^{1}H NMR (400 MHz, DMSO–d_6): 2.33 (s, 3H), 3.88 (s, 2H), 6.38 (s, 2H), 7.16–7.38 (m, 4H), 7.67 (s, 1H), 7.89 (s, 2H), 12.83 (s, 1H) (Supplementary Material Fig. S30). ^{13}C NMR (100 MHz, DMSO–d_6): 20.92 (CH_3), 40.77 (CH_2), 119.51 (CH), 120.05 (CH), 124.20 (CH), 124.37 (2C), 127.72 (2CH), 128.89 (2CH), 134.60 (C), 139.05 (C), 149.31 (C), 153.45 (C), 153.65 (C), 168.75 (C), 172.70 (C) (Supplementary Material Fig. S31). HRMS (ESI) (*m/z*) $[M + H]^+$ calcd. for $C_{18}H_{15}ClN_6OS_2$: 431.0510, found: 431.0519 (Supplementary Material Fig. S32).

*2.1.1.3.9. 2-[(4-*Amino*-5-(4-*methylphenyl*)−4H-1,2,4-*triazol*-3-*yl*)thio*]*-N-(6-bromobenzothiazol-2-yl)acetamide (**9**).* M.p.: 247–248 °C. Yield: 87%. IR ν_{max} (cm^{-1}): 3329 (N–H stretching), 3188, 3113, 3043 (Aromatic C–H stretching), 2922, 2837 (Aliphatic C–H stretching), 1681 (Amide C=O stretching), 1616, 1585, 1548, 1481 (N–H bending, C=N and C=C stretching), 1440, 1423, 1404, 1323, 1276, 1236, 1172, 1130, 1101, 1035 (C–H bending, C–N and C–O stretching, aromatic C–H in plane bending), 977, 941, 894, 881, 825, 804, 738 (Aromatic C–H out of plane bending and C-S stretching) (Supplementary Material Fig. S33). ^{1}H NMR (400 MHz, DMSO–d_6): 2.36 (s, 3H), 3.98 (s, 2H), 6.38 (s, 2H), 7.31 (d, J = 8.40 Hz, 1H), 7.35 (d, J = 8.80 Hz, 2H), 7.43 (d, J = 8.40 Hz, 1H), 7.92 (d, J = 8.00 Hz, 3H), 12.79 (s, 1H) (Supplementary Material Fig. S34). ^{13}C NMR (100 MHz, DMSO–d_6): 20.9 (CH_3), 40.7 (CH_2), 112.5 (C), 120.4 (CH), 123.0 (CH), 124.3 (CH), 124.4 (C), 127.7 (2CH), 128.9 (2CH), 134.9 (C), 139.1 (C), 149.3 (C), 153.3 (C), 153.7 (C), 167.3 (C), 171.9 (C) (Supplementary Material Fig. S35). HRMS (ESI) (*m/z*) $[M + H]^+$ calcd. for $C_{18}H_{15}BrN_6OS_2$: 475.0005, found: 475.0006 (Supplementary Material Fig. S36).

*2.1.1.3.10. 2-[(4-*Amino*-5-(4-*methylphenyl*)−4H-1,2,4-*triazol*-3-*yl*)thio*]*-N-(6-methylbenzothiazol-2-yl)acetamide (**10**).* M.p.: 206–207 °C. Yield: 90%. IR ν_{max} (cm^{-1}): 3340, 3269 (N–H stretching), 3188, 3030 (Aromatic C–H stretching), 2918 (Aliphatic C–H stretching), 1685 (Amide C=O stretching), 1598, 1558, 1481, 1456 (N–H bending, C=N and C=C stretching), 1419, 1390, 1323, 1282, 1226, 1180, 1120, 1105, 1043 (C–H bending, C–N and C–O stretching, aromatic C–H in plane bending), 999, 974, 923, 893, 815, 746, 721 (Aromatic C–H out of plane bending and C-S stretching) (Supplementary Material Fig. S37). ^{1}H NMR (400 MHz, DMSO–d_6): 2.34 (s, 3H), 2.37 (s, 3H), 3.86 (s, 2H), 6.45 (s, 2H), 7.00 (d, J = 7.60 Hz, 1H), 7.32 (t, J = 8.00, 16.00 Hz, 3H), 7.43 (s, 1H), 7.94 (d, J = 7.60 Hz, 2H), 12.81 (s, 1H) (Supplementary Material Fig. S38). ^{13}C NMR (100 MHz, DMSO–d_6): 20.8 ($2CH_3$), 40.0 (CH_2), 121.1 (CH), 124.3 (CH), 127.4 (CH), 128.3 (C), 129.6 (2CH), 130.7 (2CH), 132.1 (C), 135.9 (C), 140.9 (C), 150.2 (C), 154.3 (C), 154.5 (C), 168.2 (C), 171.8 (C) (Supplementary Material Fig. S39). HRMS (ESI) (*m/z*) $[M + H]^+$ calcd. for $C_{19}H_{18}N_6OS_2$: 411.1056, found: 411.1068 (Supplementary Material Fig. S40).

*2.1.1.3.11. 2-[(4-*Amino*-5-(4-*methylphenyl*)−4H-1,2,4-*triazol*-3-*yl*)thio*]*-N-(6-nitrobenzothiazol-2-yl)acetamide (**11**).* M.p.: 217–218 °C. Yield: 87%. IR ν_{max} (cm^{-1}): 3336, 3236 (N–H stretching), 3176, 3095 (Aromatic C–H stretching), 2922, 2837 (Aliphatic C–H stretching), 1683 (Amide C=O stretching), 1653, 1616, 1575, 1558, 1541, 1506, 1456 (N–H bending, NO_2, C=N and C=C stretching), 1435, 1321, 1280, 1224, 1166, 1124, 1045 (C–H bending, C–N and C–O stretching, aromatic C–H in plane bending), 974, 885, 819, 752, 719, 680, 651 (Aromatic C–H out of plane bending and C-S stretching) (Supplementary Material Fig. S41). ^{1}H NMR (400 MHz, DMSO–d_6): 2.35 (s, 3H), 4.13 (s, 2H), 6.25 (s, 2H), 7.28 (d, J = 6.80 Hz, 2H), 7.65 (d, J = 8.00 Hz, 1H), 7.88 (d, J = 6.40 Hz, 2H), 8.13 (d, J = 7.60 Hz, 1H), 8.73 (s, 1H), 12.80 (s, 1H) (Supplementary Material Fig. S42). ^{13}C NMR (100 MHz, DMSO–d_6): 20.8 (CH_3), 38.3 (CH_2), 117.8 (CH), 118.8 (CH), 121.0 (CH), 124.1 (C), 127.6 (2CH), 128.9 (2CH), 132.7 (C), 139.2 (C), 141.3 (C), 153.0 (C), 153.9 (C), 155.3 (C), 169.4 (C), 172.0 (C) (Supplementary Material Fig. S43). HRMS (ESI) (*m/z*) $[M + H]^+$ calcd. for $C_{18}H_{15}N_7O_3S_2$: 442.0751, found: 442.0772 (Supplementary Material Fig. S44).

*2.1.1.3.12. 2-[(4-*Amino*-5-(4-*methylphenyl*)−4H-1,2,4-*triazol*-3-*yl*)thio*]*-N-(5-nitrothiazol-2-yl)acetamide (**12**).* M.p.: 182–183 °C. Yield: 65%. IR ν_{max} (cm^{-1}): 3361, 3282 (N–H stretching), 3095, 3043 (Aromatic C–H stretching), 2924, 2837 (Aliphatic C–H stretching), 1672 (Amide C=O stretching), 1612, 1575, 1537, 1456 (N–H bending, NO_2, C=N and C=C stretching), 1413, 1381, 1321, 1288, 1244, 1182, 1145, 1120, 1101, 1045 (C–H bending, C–N and C–O stretching, aromatic C–H in plane bending), 962, 906, 819, 742, 719 (Aromatic C–H out of plane bending and C-S stretching) (Supplementary Material Fig. S45). ^{1}H NMR (400 MHz, DMSO–d_6): 2.37 (s, 3H), 4.03 (s, 2H), 6.27 (s, 2H), 7.31 (d, J = 8.40 Hz, 2H), 7.91 (d, J = 8.00 Hz, 2H), 8.44 (s, J = 7.60 Hz, 1H), 12.76 (s, 1H) (Supplementary Material Fig. S46). ^{13}C NMR (100 MHz, DMSO–d_6): 20.8 (CH_3), 38.3 (CH_2), 124.2 (C), 127.6 (2CH), 128.8 (2CH), 136.3 (C), 139.0 (C), 145.7 (CH), 153.0 (C), 153.7 (C), 173.1 (C), 175.0 (C) (Supplementary Material Fig. S47). HRMS (ESI) (*m/z*) $[M + H]^+$ calcd. for $C_{14}H_{13}N_7O_3S_2$: 392.0594, found: 392.0592 (Supplementary Material Fig. S48).

*2.1.1.3.13. 2-[(4-*Amino*-5-(3-*pyridyl*)−4H-1,2,4-*triazol*-3-*yl*)*thio*]-N-(benzothiazol-2-yl)acetamide (**13**) (CAS registry number 901,151–99–3).* M.p.: 221–222 °C. Yield: 62%. IR ν_{max} (cm^{-1}): 3317 (N–H stretching), 3172, 3062 (Aromatic C–H stretching), 2924, 2848 (Aliphatic C–H stretching), 1681 (Amide C=O stretching), 1633, 1598, 1568, 1548, 1504, 1483 (N–H bending, C=N and C=C stretching), 1440, 1392, 1323, 1267, 1226, 1174, 1124, 1026 (C–H bending, C–N and C–O stretching, aromatic C–H in plane bending), 975, 937, 879, 812, 752, 698, 680 (Aromatic C–H out of plane bending and C-S stretching) (Supplementary Material Fig. S49). ^{1}H NMR (400 MHz, DMSO–d_6): 4.32 (s, 2H), 6.32 (s, 2H), 7.29 (t, J = 8.00, 7.60, 15.60 Hz, 1H), 7.42 (t, J = 7.60, 15.20 Hz, 1H), 7.54–7.57 (m, 1H), 7.75 (d, J = 8.40 Hz, 1H), 7.94 (d, J = 8.00 Hz, 1H), 8.36 (d, J = 8.40 Hz, 1H), 8.69 (s, 1H), 9.16 (s, 1H), 12.60 (s, 1H) (Supplementary Material Fig. S50). ^{13}C NMR (100 MHz, DMSO–d_6): 35.3 (CH_2), 120.4 (CH), 121.5 (CH), 123.0 (CH), 123.3 (CH), 123.5 (CH), 125.9 (C), 131.5 (C), 135.0 (CH), 148.1 (C), 148.6 (CH), 150.3 (CH), 152.2 (C), 153.6 (C), 158.5 (C), 167.7 (C) (Supplementary Material Fig. S51). HRMS (ESI) (m/z) $[M + H]^+$ calcd. for $C_{16}H_{13}N_7OS_2$: 384.0696, found: 384.0696 (Supplementary Material Fig. S52).

*2.1.1.3.14. 2-[(4-*Amino*-5-(3-*pyridyl*)−4H-1,2,4-*triazol*-3-*yl*)*thio*]-N-(6-chlorobenzothiazol-2-yl)acetamide (**14**).* M.p.: 258–259 °C. Yield: 82%. IR ν_{max} (cm^{-1}): 3315 (N–H stretching), 3140, 3061 (Aromatic C–H stretching), 2958, 2922, 2837 (Aliphatic C–H stretching), 1660 (Amide C=O stretching), 1597, 1564 (N–H bending, C=N and C=C stretching), 1446, 1421, 1379, 1330, 1255, 1228, 1178, 1128, 1095, 1026 (C–H bending, C–N and C–O stretching, aromatic C–H in plane bending), 972, 921, 866, 800, 761, 746, 704 (Aromatic C–H out of plane bending and C-S stretching) (Supplementary Material Fig. S53). ^{1}H NMR (400 MHz, DMSO–d_6): 4.33 (s, 2H), 6.29 (s, 2H), 7.45 (d, J = 6.80 Hz, 1H), 7.54–7.57 (m, 1H), 7.75 (d, J = 8.40 Hz, 1H), 8.10 (s, 1H), 8.35 (d, J = 7.60 Hz, 1H), 8.52 (s, 1H), 9.14 (s, 1H), 12.62 (s, 1H) (Supplementary Material Fig. S54). ^{13}C NMR (100 MHz, DMSO–d_6): 34.8 (CH_2), 121.2 (CH), 121.6 (CH), 122.9 (CH), 123.4 (CH), 126.3 (C), 127.4 (C), 133.1 (C), 134.9 (CH), 147.3 (C), 148.0 (CH), 150.3 (CH), 152.2 (C), 153.4 (C), 158.8 (C), 167.7 (C) (Supplementary Material Fig. S55). HRMS (ESI) (m/z) $[M + H]^+$ calcd. for $C_{16}H_{12}ClN_7OS_2$: 418.0306, found: 418.0312 (Supplementary Material Fig. S56).

*2.1.1.3.15. 2-[(4-*Amino*-5-(3-*pyridyl*)−4H-1,2,4-*triazol*-3-*yl*)*thio*]-N-(6-bromobenzothiazol-2-yl)acetamide (**15**) (CAS registry number 901,615–40–5).* M.p.: 261–262 °C. Yield: 83%. IR ν_{max} (cm^{-1}): 3315 (N–H stretching), 3143, 3057 (Aromatic C–H stretching), 2960, 2927, 2831 (Aliphatic C–H stretching), 1660 (Amide C=O stretching), 1597, 1562, 1487 (N–H bending, C=N and C=C stretching), 1444, 1419, 1377, 1330, 1257, 1226, 1176, 1128, 1083, 1026 (C–H bending, C–N and C–O stretching, aromatic C–H in plane bending), 974, 923, 840, 800, 742, 704, 680 (Aromatic C–H out of plane bending and C-S stretching) (Supplementary Material Fig. S57). ^{1}H NMR (400 MHz, DMSO–d_6): 4.34 (s, 2H), 6.29 (s, 2H), 7.54–7.59 (m, 2H), 7.70 (d, J = 8.80 Hz, 1H), 8.24 (s, 1H), 8.35 (d, J = 8.00 Hz, 1H), 8.69 (d, J = 6.40 Hz, 1H), 9.14 (s, 1H), 12.76 (s, 1H) (Supplementary Material Fig. S58). ^{13}C NMR (100 MHz, DMSO–d_6): 34.7 (CH_2), 115.4 (CH), 122.1 (C), 122.9 (CH), 123.4 (CH), 124.1 (CH), 129.0 (C), 133.6 (C), 134.9 (CH), 147.6 (C), 148.0 (CH), 150.3 (CH), 152.2 (C), 153.5 (C), 158.5 (C), 167.6 (C) (Supplementary Material Fig. S59). HRMS (ESI) (m/z) $[M + H]^+$ calcd. for $C_{16}H_{12}BrN_7OS_2$: 461.9801, found: 461.9810 (Supplementary Material Fig. S60).

*2.1.1.3.16. 2-[(4-*Amino*-5-(3-*pyridyl*)−4H-1,2,4-*triazol*-3-*yl*)*thio*]-N-(6-methylbenzothiazol-2-yl)acetamide (**16**).* M.p.: 252–253 °C. Yield: 76%. IR ν_{max} (cm^{-1}): 3311 (N–H stretching), 3151, 3053 (Aromatic C–H stretching), 2956, 2922, 2843 (Aliphatic C–H stretching), 1656 (Amide C=O stretching), 1610, 1573, 1456 (N–H bending, C=N and C=C stretching), 1421, 1377, 1336, 1253, 1226, 1178, 1128, 1028 (C–H bending, C–N and C–O stretching, aromatic C–H in plane bending), 972, 898, 866, 800, 748, 704, 682, 661 (Aromatic C–H out of plane bending and C-S stretching) (Supplementary Material Fig. S61). ^{1}H NMR (400 MHz, DMSO–d_6): 2.40 (s, 3H), 4.33 (s, 2H), 6.29 (s, 2H), 7.25 (d, J = 8.00 Hz, 1H), 7.54–7.57 (m, 1H), 7.65 (d, J = 8.80 Hz, 1H), 7.75 (s, 1H), 8.35 (d, J = 8.40 Hz, 1H), 8.69 (s, 1H), 9.15 (s, 1H), 12.57 (s, 1H) (Supplementary Material Fig. S62). ^{13}C NMR (100 MHz, DMSO–d_6): 20.8 (CH_3), 34.7 (CH_2), 120.1 (CH), 121.1 (CH), 122.9 (CH), 123.4 (CH), 127.4 (C), 131.5 (C), 133.0 (C), 134.9 (CH), 146.4 (C), 148.1 (CH), 150.3 (CH), 152.2 (C), 153.5 (C), 156.8 (C), 167.1 (C) (Supplementary Material Fig. S63). HRMS (ESI) (m/z) $[M + H]^+$ calcd. for $C_{17}H_{15}N_7OS_2$: 398.0852, found: 398.0860 (Supplementary Material Fig. S64).

*2.1.1.3.17. 2-[(4-*Amino*-5-(3-*pyridyl*)−4H-1,2,4-*triazol*-3-*yl*)*thio*]-N-(6-nitrobenzothiazol-2-yl)acetamide (**17**).* M.p.: 232–233 °C. Yield: 82%. IR ν_{max} (cm^{-1}): 3338, 3280 (N–H stretching), 3165, 3105 (Aromatic C–H stretching), 2968, 2924, 2900 (Aliphatic C–H stretching), 1668 (Amide C=O stretching), 1612, 1575, 1556, 1506 (N–H bending, NO_2, C=N and C=C stretching), 1435, 1392, 1323, 1278, 1261, 1228, 1168, 1122, 1043 (C–H bending, C–N and C–O stretching, aromatic C–H in plane bending), 972, 891, 846, 827, 812, 752, 702 (Aromatic C–H out of plane bending and C-S stretching) (Supplementary Material Fig. S65). ^{1}H NMR (400 MHz, DMSO–d_6): 4.29 (s, 2H), 6.33 (s, 2H), 7.54–7.57 (m, 1H), 7.80 (d, J = 9.20 Hz, 1H), 8.22 (d, J = 8.40 Hz, 1H), 8.36 (d, J = 8.00 Hz, 1H), 8.68 (s, 1H), 8.91 (s, 1H), 9.15 (s, 1H), 12.57 (s, 1H) (Supplementary Material Fig. S66). ^{13}C NMR (100 MHz, DMSO–d_6): 36.3 (CH_2), 120.1 (CH), 119.8 (CH), 121.3 (CH), 123.0 (CH), 123.4 (C), 132.4 (C), 134.9 (CH), 142.2 (C), 148.1 (C), 150.3 (CH), 152.1 (CH), 153.6 (C), 154.2 (C), 166.0 (C), 169.8 (C) (Supplementary Material Fig. S67). HRMS (ESI) (m/z) $[M + H]^+$ calcd. for $C_{16}H_{12}N_8O_3S_2$: 429.0547, found: 429.0549 (Supplementary Material Fig. S68).

*2.1.1.3.18. 2-[(4-*Amino*-5-(3-*pyridyl*)−4H-1,2,4-*triazol*-3-*yl*)*thio*]-N-(5-nitrothiazol-2-yl)acetamide (**18**).* M.p.: 181–182 °C. Yield: 52%. IR ν_{max} (cm^{-1}): 3325, 3224 (N–H stretching), 3151, 3078 (Aromatic C–H stretching), 2926, 2833 (Aliphatic C–H stretching), 1687 (Amide C=O stretching), 1633, 1593, 1573, 1492 (N–H bending, NO_2, C=N and C=C stretching), 1429, 1384, 1355, 1294, 1251, 1186, 1138, 1118, 1026 (C–H bending, C–N and C–O stretching, aromatic C–H in plane bending), 968, 894, 821, 738, 700, 659, 628 (Aromatic C–H out of plane bending and C-S stretching) (Supplementary Material Fig. S69). ^{1}H NMR (400 MHz, DMSO–d_6): 4.09 (s, 2H), 6.39 (s, 2H), 7.54–7.58 (m, 1H), 8.38 (d, J = 7.60 Hz, 1H), 8.47 (s, 1H), 8.68 (d, J = 6.40 Hz, 1H), 9.15 (s, 1H), 12.63 (s, 1H) (Supplementary Material Fig. S70). ^{13}C NMR (100 MHz, DMSO–d_6): 38.5 (CH_2), 123.2 (CH), 123.5 (C), 135.1 (CH), 136.8 (C), 145.7 (CH), 148.2 (CH), 150.3 (CH), 151.9 (C), 154.1 (C), 172.5 (C), 174.5 (C) (Supplementary Material Fig. S71). HRMS (ESI) (m/z) $[M + H]^+$ calcd. for $C_{12}H_{10}N_8O_3S_2$: 379.0390, found: 379.0390 (Supplementary Material Fig. S72).

2.2. Biochemistry

2.2.1. AR activity assay

AR activity was assessed by means of the absorbance decrease of NADPH at 340 nm spectrophotometrically. Enzymatic reaction mixture (1 mL total volume) contains 0.1 M sodium phosphate buffer (pH = 5.5), 4.7 mM DL-glyceraldehyde, 0.11 mM NADPH and enzyme solution [41].

2.2.2. Homogenate preparation and purification of AR from bovine liver

The homogenate was centrifuged at 13.500 x g for 60 min after approximately 15 g of bovine liver was homogenized in 45 mL of 10 mM sodium phosphate buffer (pH = 7.4). The supernatant was used for the next experiments. The supernatant suspension was precipitated with ammonium sulfate. The precipitation intervals for AR were detected as 0%−70%. The precipitate was gath-

ered by centrifugation at 13.500 × *g* for 30 min and redissolved in a 10 mM sodium phosphate buffer (pH = 7.4). The solution was dialyzed against 10 mM sodium phosphate buffer (pH = 7.4) containing 5 mM 2-mercaptoethanol.

The dialyzed enzyme solution was loaded onto the DE-52 cellulose anion exchange column formerly equilibrated with 10 mM sodium phosphate buffer (pH= 7.4). AR was not allowed to attach to the column at pH = 7.4 and left the column with the same buffer. The purpose herein was to separate AR from other enzymes attached to the column. The fractions were collected, and the enzyme activity was controlled at 340 nm. After the fractions displaying the enzyme activity were pooled and mixed with glycerol (10%), this enzyme solution was loaded onto the Sephadex G-100 column equilibrated with 10 mM sodium phosphate buffer (pH = 7.4). The fractions were analyzed for both protein amount (at 280 nm) and enzyme activity (at 340 nm). Then, the fractions from the Sephadex G-100 column were loaded onto the 2′,5′-ADP Sepharose 4B affinity column equilibrated with 10 mM sodium phosphate buffer (pH = 7.4). The column was washed with 10 mM sodium phosphate buffer (pH = 7.4) and then elution was performed with linear gradient of 50–250 mM NaCl. The enzyme activity was controlled at 340 nm in collected fractions, and the tubes showing enzyme activity were combined. All purification steps were performed at 4 °C [42].

2.2.3. Protein determination

During the purification steps, Bradford method was used to determine the quantitative protein by measuring the absorbance at 595 nm using bovine serum albumin as a standard [43].

2.2.4. Sodium dodecyl sulfate-polyacrylamide gel electrophoresis (SDS-PAGE)

The enzyme purity was checked according to Laemmli's procedure [44]. This method consists of 3% and 8% acrylamide concentrations for running and stacking gel, respectively according to previous studies [45–47]. SDS-PAGE gel was stained with silver and the electrophoretic pattern was photographed.

2.2.5. In vitro *inhibition studies*

The AR activity was measured in the presence of different concentrations of compounds **1**–**18**. Half maximal inhibitory concentration (IC_{50}) was defined as the concentration of compound causing 50% inhibition and it was calculated from Activity%-[Compounds] graphs for each compound [48–50]. In order to determine the V_{max} and K_m values for the enzyme, activity measurements were performed at five different concentrations of DL-glyceraldehyde (0.070, 0.141, 0.230, 0.320 and 0.420 mM) and Lineweaver–Burk graphs were plotted [51] according to the previous studies [52–54]. The inhibition types and inhibition constant (K_i) values were found from graphs with three different concentrations of tested compounds. All measurements were repeated three times.

2.2.6. Statistical analyses

Analysis of the data, calculation of IC_{50} and K_i values, and drawing of graphs were carried out using GraphPad Prism 7 software. Differences between data sets were examined using the Kruskal-Wallis test and considered statistically significant when the p-value was less than 0.05. For significant p-values, post hoc Dunn's multiple comparisons tests were performed. The K_i constants were presented as mean ± standard deviation (95% confidence intervals).

2.3. Cytotoxicity studies

2.3.1. Cell culture and drug treatment

L929 mouse fibroblast cells were incubated in 90% DMEM, supplemented with 10% fetal bovine serum (Gibco, Paisley, Scotland) and 100 IU/mL penicillin-streptomycin (Gibco, Paisley, Scotland) and 1% glutamin. Then, cells were incubated at 37 °C in a humidified atmosphere of 95% air and 5% CO_2. Exponentially growing cells were plated at 2×10^4 cells/mL into 96-well microtiter tissue culture plates (Nunc, Roskilde, Denmark). The optimum cell number for cytotoxicity assays was determined in preliminary experiments. The stock solutions of the compounds were prepared in DMSO and further dilutions were made with a fresh culture medium (the concentration of DMSO in the final culture medium was 0.1% which had no effect on the cell viability) [37].

2.3.2. MTT assay

The level of cellular 3-(4,5-dimethylthiazol-2-yl)−2,5-diphenyltetrazolium bromide (MTT) reduction was quantified as previously described in the literature [55] with small modifications [37]. L929 cells (2×10^4 cells/mL) were seeded on 96-well plates and incubated for 24 h at 37 °C. Then, the tested compounds were added to give final concentration in the range of 0.195–25 µM and the cells were incubated for 24 h. At the end of this period, MTT was added to final concentration of 0.5 μg/mL and the cells were incubated for 2 h at 37 °C. After removal of medium, the formazan crystals formed by MTT metabolism were solubilized by the addition of 200 μL DMSO to each well and absorbance was read at 540 nm with a microplate spectrophotometer (Bio-Tek, Winooski, VT, USA). Every concentration was repeated in three wells and the IC_{50} values (μM) for cell viability were defined as the concentrations of compounds that reduced absorbance to 50% of control (untreated cells) values and represented as mean ±SD.

2.4. In silico studies

2.4.1. Molecular docking studies

The X-ray crystallographic structure of AR was obtained from the PDB server (PDB ID code: 1T41) [37,56] and optimized for docking studies in protein preparation module of Schrödinger software (Schrödinger Release 2016–2: Schrödinger, LLC, New York, NY, USA). Ligands were prepared with energy minimization using Optimized Potential Liquid Simulations (OPLS_2005) force field at physiological pH in ligand preparation module of Schrödinger software. In molecular docking simulations: Grid Generation and Glide/XP docking protocols were applied for the prediction of topologies of compounds **1**–**18**, quercetin and sorbinil in the active site of AR [37].

2.4.2. ADME prediction

Some physicochemical properties and the bioavailability of compounds **1**–**18** were predicted by QikProp module of Schrödinger software (Schrödinger Release 2016–2: QikProp, Schrödinger, LLC, New York, NY, 2016). This module computes physically significant descriptors and pharmaceutically relevant properties compared to the determined range or recommended values.

3. Results and discussion

3.1. Chemistry

In this work, the synthesis of the desired new triazoles (**1**–**18**) was accomplished as described in Scheme 1. Initially, 4-amino-5-aryl-*4H*-1,2,4-triazole-3-thiol (**A**) was synthesized *via* the reaction of 5-aryl-1,3,4-oxadiazole-2-thiol with hydrazine hydrate [38]. Meanwhile, 2–chloro–*N*-(thiazol/benzothiazol-2-yl)acetamide derivatives were obtained *via* the reaction of 2-aminothiazoles/benzothiazoles with chloroacetyl chloride

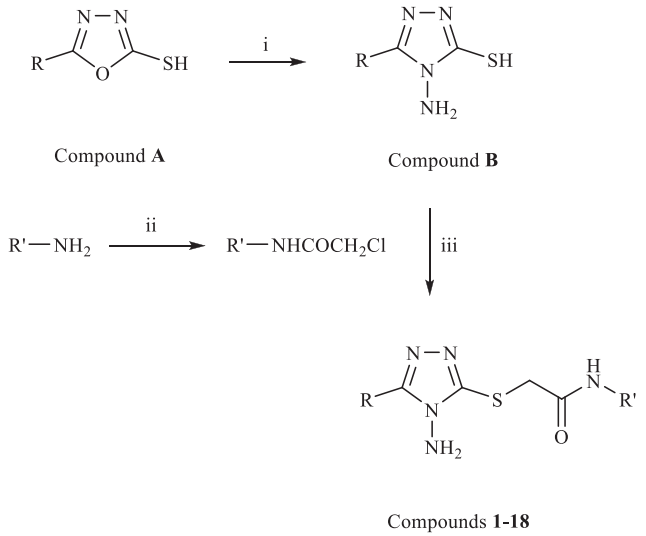

Compound	R	R'
1	4-Methoxyphenyl	Benzothiazol-2-yl
2	4-Methoxyphenyl	6-Chlorobenzothiazol-2-yl
3	4-Methoxyphenyl	6-Bromobenzothiazol-2-yl
4	4-Methoxyphenyl	6-Methylbenzothiazol-2-yl
5	4-Methoxyphenyl	6-Nitrobenzothiazol-2-yl
6	4-Methoxyphenyl	5-Nitrothiazol-2-yl
7	4-Methylphenyl	Benzothiazol-2-yl
8	4-Methylphenyl	6-Chlorobenzothiazol-2-yl
9	4-Methylphenyl	6-Bromobenzothiazol-2-yl
10	4-Methylphenyl	6-Methylbenzothiazol-2-yl
11	4-Methylphenyl	6-Nitrobenzothiazol-2-yl
12	4-Methylphenyl	5-Nitrothiazol-2-yl
13	3-Pyridyl	Benzothiazol-2-yl
14	3-Pyridyl	6-Chlorobenzothiazol-2-yl
15	3-Pyridyl	6-Bromobenzothiazol-2-yl
16	3-Pyridyl	6-Methylbenzothiazol-2-yl
17	3-Pyridyl	6-Nitrobenzothiazol-2-yl
18	3-Pyridyl	5-Nitrothiazol-2-yl

Scheme 1. The synthetic route for the preparation of compounds **1–18**. Reagents and conditions: (i) $NH_2NH_2.H_2O$, ethanol, reflux, 12 h; (ii) $ClCOCH_2Cl$, TEA, toluene, 0–5 °C; (iii) K_2CO_3, acetone, rt, 8 h.

in the presence of TEA [39]. Then, the subsequent nucleophilic substitution reaction of compound **A** with 2–chloro–*N*-(thiazol/benzothiazol-2-yl)acetamides in the presence of potassium carbonate led to the formation of the target compounds (**1–18**).

The structures of title compounds (**1–18**) were verified by different spectroscopic techniques, such as Infrared (IR), ^{1}H Nuclear Magnetic Resonance (NMR), ^{13}C NMR and High Resolution Mass Spectrometry (HRMS). In the IR spectra of compounds **1–18**, the N–H stretching bands belonging to the amino group at the 4th position of 1,2,4-triazole scaffold and the acetamide group were observed at 3211–3381 cm^{-1} as expected [39,40]. The amide C=O stretching bands appearing at 1656–1693 cm^{-1} confirmed the formation of the final compounds. Moreover, the aromatic and aliphatic C–H stretching vibrations gave rise to the bands at 3003–3188 cm^{-1} and 2831–2999 cm^{-1}, respectively. The C=N, C=C stretching and N–H bending bands were detected at 1456–1653 cm^{-1}. Finally, the C–H bending, C–N and C–O stretching, aromatic C–H in plane and out of plane bending and C-S stretching bands occurred at prospective regions.

In the ^{1}H NMR spectra of compounds **1–18**, the observation of the characteristic singlet peaks at 3.86–4.34 ppm and 12.56–12.83 ppm of S-CH_2 and NH protons, respectively is a clear evidence for the formation of the thioacetamides of final compounds. Along with this data, the singlet NH_2 protons belonging to 1,2,4-triazoles appeared at 5.77–6.45 ppm. In the ^{1}H NMR spectra of compounds **1–18**, the singlet peak belonging to the methoxy protons attached to the phenyl moiety of compounds **1–6** was detected at 3.77–3.81 ppm, whereas the singlet peak belonging to the methyl protons attached to the phenyl moiety of compounds **7–12** became apparent at 2.33–2.37 ppm. Moreover, the singlet peak belonging to the methyl protons at the 6th position of benzothiazole scaffold present in compounds **4, 10** and **16** emanated at 2.34–2.40 ppm. All other aromatic and heteroaromatic protons were consistent with the proposed structures of the compounds. In the ^{13}C NMR spectra of compounds **1–18**, the important S-CH_2 and C=O carbons at 34.7–40.7 ppm and 167.1–175.0 ppm, respectively also substantiated the formation of the thioacetamide moieties of final compounds. The methoxy carbons of compounds **1–6** and the methyl carbons at the 4th position of the phenyl ring of compounds **7–12** came in sight at 55.2–55.3 ppm and 20.8–20.9 ppm, respectively. Besides, the methyl carbons of the 6-methylbenzothiazoles of compounds **4, 10** and **16** appeared at 20.8–20.9 ppm. The C_3 and C_5 carbons of triazoles gave rise to peaks at 153.0–155.7 ppm and 151.9–154.3 ppm, respectively. All other carbon peaks belonging to benzothiazole, thiazole, phenyl and pyridine scaffolds also approved the proposed structures of the final compounds. Once and for all, the HRMS data of compounds **1–18** matched with their molecular formulas.

3.2. Biochemistry

In this study, diverse chromatographic methods, namely DE-52 cellulose anion exchange chromatography, Sephadex G-100 gel filtration chromatography and 2′,5′-ADP-Sepharose 4B affinity column chromatography were applied to purify AR from bovine liver. It was purified 338.98-fold with a yield of 1.12% and a specific activity of 1.70 EU/mg (Table 1). SDS-PAGE was performed to check the purity of AR and a single band at around 39 kDa was observed (Fig. 3). Both the IC_{50} and the K_i values of compounds **1–18** were obtained from the Activity%-[Inhibitor] and Lineweaver-Burk (1/V-1/[S]) graphs, respectively. The inhibition types of compounds **1–18** as competitive or non-competitive inhibition were also determined

Table 1
Summary of the AR purification procedure.

Purification Steps	Activity (EU/mL)	Total volume (mL)	Protein (mg/mL)	Total protein (mg)	Total activity (EU)	Specific activity (EU/mg)	Yield (%)	Purification fold
Homogenate	0.265	40	32.44	1297.60	10.60	0.0081	100	1
Ammonium sulfate precipitation and dialysis	0.285	30	21.13	633.90	8.55	0.0135	80.66	1.67
DE-52 Cellulose anion exchange chromatography	0.180	24	7.22	173.28	4.32	0.0249	40.75	3.07
Sephadex G-100 gel filtration chromatography	0.085	10	0.102	1.02	0.85	0.8333	8.02	102.88
2′,5′-ADP-Sepharose 4B Affinity chromatography	0.017	7	0.010	0.070	0.119	1.70	1.12	209.88

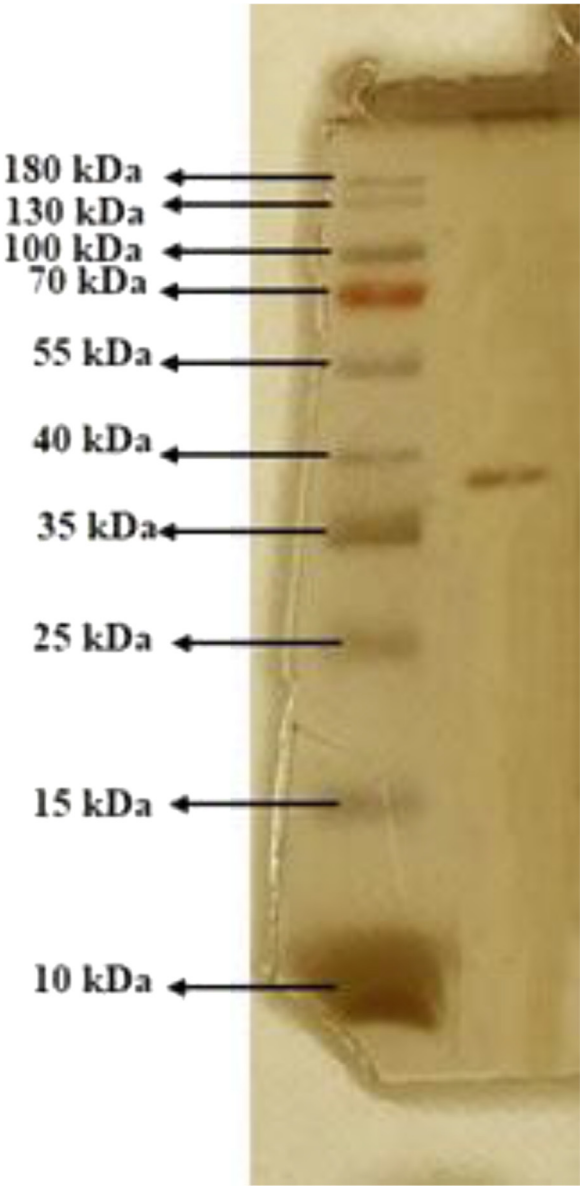

Fig. 3. The SDS-PAGE analysis of purified AR.

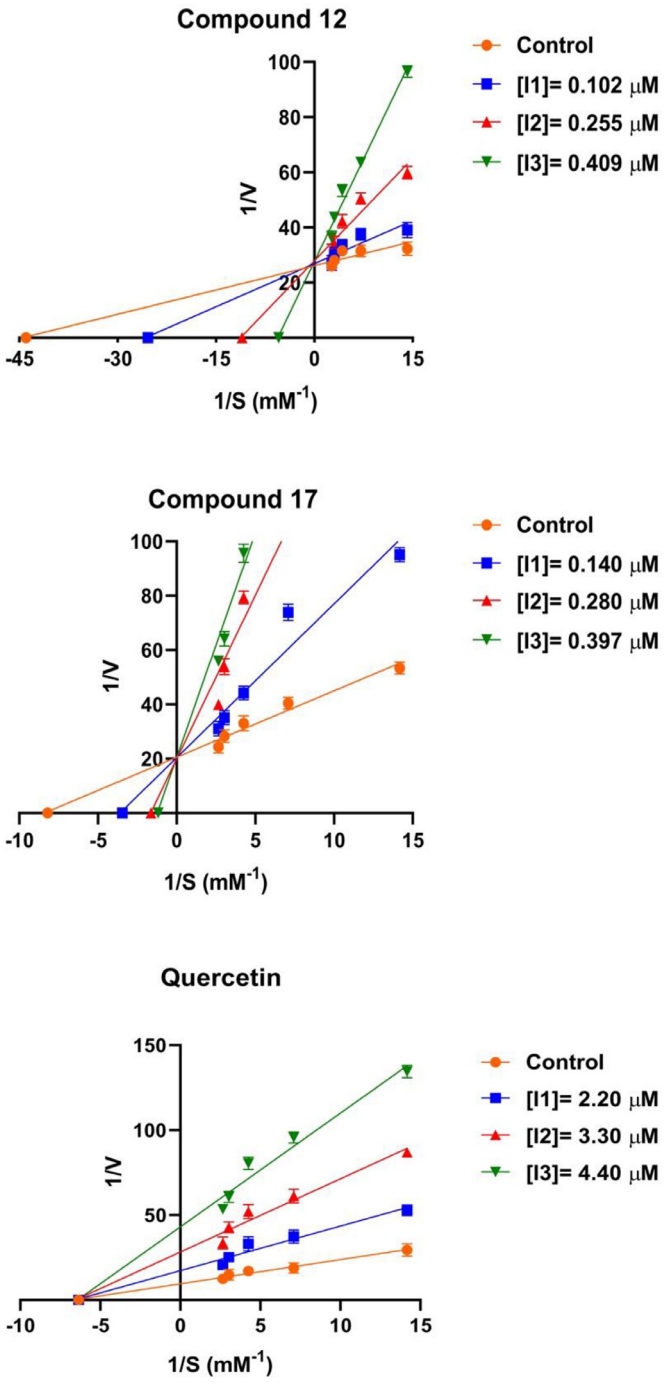

Fig. 4. The Lineweaver-Burk plots of compounds **12, 17** and quercetin (All measurements were repeated three times).

[57,58]. Competitive inhibition is proportional to the amount of inhibitor bound in the active site and is therefore proportional to inhibitor concentration. Because the inhibitor binds reversibly, the substrate can compete with it at high substrate concentrations. Thus a competitive inhibitor does not change the V_{max} of an enzyme. On the other hand, competitive inhibitors raise the K_m of an enzyme since higher concentrations of substrate would be required to achieve half-maximal activity. Non-competitive inhibition is a type of enzyme inhibition where the inhibitor reduces the activity of the enzyme and binds equally well to the enzyme whether or not it has already bound the substrate. When a non-competitive inhibitor is added the V_{max} is changed, while the K_m remains unchanged. According to the Lineweaver-Burk plot the V_{max} is reduced during the addition of a non-competitive inhibitor, which is shown in the plot by a change in both the slope and y-intercept when a non-competitive inhibitor is added. K_m and V_{max} values were determined for competitive and non-competitive inhibition. K_m values were found as 10.04 and 17.20 mM for non-competitive and competitive inhibition respectively. V_{max} values were found as 0.056 and 0.035 mM/min for non-competitive and competitive inhibition, respectively. Quercetin was used as a standard AR inhibitor depending on relevant studies [59–61].

K_i denotes the equilibrium constant of the dissociation of the inhibitor-bound enzyme complex, whereas IC_{50} quantifies the concentration of inhibitor necessary to halve the reaction rate of an enzyme-catalyzed reaction observed under specified assay conditions. Since K_i is an important constant associated with enzyme kinetics, the AR inhibitory effects of compounds **1**–**18** were compared based on their K_i values [62]. The results indicated that the compounds displayed excellent AR inhibitory activity according to the IC_{50} and the K_i values in the range of 0.205 μM-0.346 μM and 0.04 ± 0.01 μM–0.81 ± 0.11 μM, respectively when com-

Table 3
The IC_{50} values of compounds **1–18** on L929 cell line for 24 h.

Compound	IC_{50} (μM)	Compound	IC_{50} (μM)
1	10.67 ± 1.53	**10**	0.58 ± 0.03
2	>25	**11**	11.5 ± 1.73
3	>25	**12**	1.07 ± 1.12
4	>25	**13**	<0.195
5	>25	**14**	<0.195
6	7.5 ± 1.32	**15**	<0.195
7	10.67 ± 1.53	**16**	<0.195
8	>25	**17**	20.5 ± 0.71
9	>25	**18**	6.55 ± 1.34

Table 4
Docking score (kcal/mol), glide gscore (kcal/mol) and glide emodel (kcal/mol) results of compounds **1–18** for AR (PDB ID code: 1T41).

Compound	1T41		
	Docking score	Glide score	Glide emodel
1	−4.99	−6.74	−47.82
2	−4.76	−6.41	−44.43
3	−6.41	−6.48	−35.55
4	−4.34	−4.38	−47.14
5	−4.88	−6.18	−39.24
6	−4.20	−5.85	−45.86
7	−4.88	−6.18	−39.24
8	−2.91	−2.94	−32.09
9	−3.22	−3.33	−47.14
10	−1.81	−3.56	−42.04
11	−4.64	−5.95	−37.80
12	−6.74	−6.78	−39.59
13	−2.68	−2.71	−36.48
14	−5.65	−5.72	−31.79
15	−5.61	−6.66	−46.84
16	−5.81	−7.50	−50.37
17	−6.61	−6.64	−33.57
18	−6.13	−6.20	−35.55
Quercetin	−6.34	−8.68	−43.64
Sorbinil	−5.94	−6.59	−46.80

pared to quercetin (IC_{50} = 3.86 μM and K_i = 5.66 ± 0.66 μM) (Table 2). The inhibitory potencies varied with the modifications at the 5th position of the triazole and *N*-(substituted)acetamide moieties. 4-Methylphenyl and 5-nitrothiazole carrying compound (**12**) and 3-pyridyl and 6-nitrobenzothiazole substituted compound (**17**) were found as the most potential AR inhibitors in this series with the K_i values of 0.04±0.01 μM and 0.08±0.02 μM, respectively. These compounds showed competitive inhibition behaviours against AR (Fig. 4). Aside from compounds **12** and **17**, compounds **3, 6, 14** and **15** exhibited competitive inhibition in this series. 4-Methylphenyl and 6-methylbenzothiazole bearing compound (**10**) was determined to exhibit the lowest AR inhibitory activity with the K_i value of 0.81±0.11 μM indicating that two methyl moieties substituted at the exact opposite sides together diminished the AR inhibitory potency. Compounds **12** and **17** were also identified as the most significant AR inhibitors among compounds **7–12** and compounds **13–18**, respectively. In the same manner, among compounds **1–6**, compound **3** showed the most obvious enhancement in AR inhibition with the K_i value of 0.19 ± 0.01 μM.

One of the most significant drawback to available AR inhibitors is toxicity and untoward side effects. Therefore, the cytotoxic effects of compounds **1–18** on L929 mouse fibroblast (healthy) cell line were evaluated using MTT assay. Compounds **10, 13, 14, 15** and **16** were determined as toxic at their effective concentrations. This outcome indicated that the existence of 3-pyridyl moiety led to an increase in cytotoxicity to healthy cells apart from compounds **17** and **18** (Table 3). On the other hand, other compounds exerted no cytotoxicity towards L929 cells at their IC_{50} values determined for their AR inhibitory activities pointing out their safety as AR inhibitors.

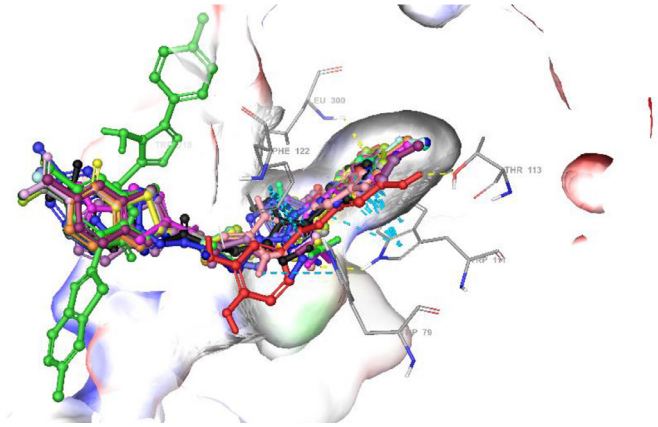

Fig. 5. Docking poses of compounds **1–18** along with quercetin and sorbinil in the active site of AR (Blue and green dashes: π-π interactions, yellow dashes: hydrogen bonding).

3.3. Molecular docking studies

In an attempt to understand the mechanistic details of biological activity, molecular docking studies were employed for compounds **1–18** along with quercetin and sorbinil in the active site of AR (PDB ID code: 1T41) [37,56]. Highly hydrophobic active site pocket of AR consists of residues such as Trp20, Trp79, Trp111, Trp219, Phe122 and Leu300 [63,64]. In general, compounds **1–18** displayed high affinity forming proper interactions and only compound **10** formed no observable intermolecular interactions (Fig. 5). Compounds **1–18**, excluding compound **10**, presented π-π stacking interactions with Trp219 and Phe122 through their triazole moieties. The substitutions at 5th position of the triazole ring also played a crucial role in the formation of π-π stacking interactions with Trp111. *N*-(substituted)acetamide moieties were engaged with water molecules *via* hydrogen bonds. Quercetin and sorbinil exhibited π-π stacking interactions with Trp111 but they missed key interactions with Trp219 and Phe122. The docked pose and interactions of compounds **12** and **17** were depicted in detail in Fig. 6. In order to compare the different conformations of the same ligand, the emodel score is generally preferred, while the different ligands are compared using the docking score [65]. All docking scores of the compounds were determined to range from −2.68 to −6.74 kcal/mol. In general, the docking scores of compounds were consistent with the biological data. The lowest docking score, belonging to compound **10** explained its low inhibitory potency and binding capacity to the active site of AR. The docking scores of compounds **12** and **17** were calculated as −6.74 and −6.61 kcal/mol as compared to quercetin (−6.34 kcal/mol) and sorbinil (−5.94 kcal/mol) (Table 4).

3.4. In silico *ADME studies*

The Absorption, Distribution, Metabolism and Excretion (ADME) profiles of compounds **1–18** were predicted by means of QikProp, a predictive ADME module within the Maestro suite produced by Schrödinger (Table 5). The conformation-independent predicted aqueous solubility (CIQPlogS), brain/blood partition coefficient (QPlogBB), human serum albumin binding (QPlogKhsa), predicted octanol/water partition coefficient (QPlogPo/w) of all compounds were found within the acceptable range. The compliance of compounds **1–18** to Lipinski's rule of five and Jorgensen's rule of three was also investigated. Lipinski's rule of five states that drug

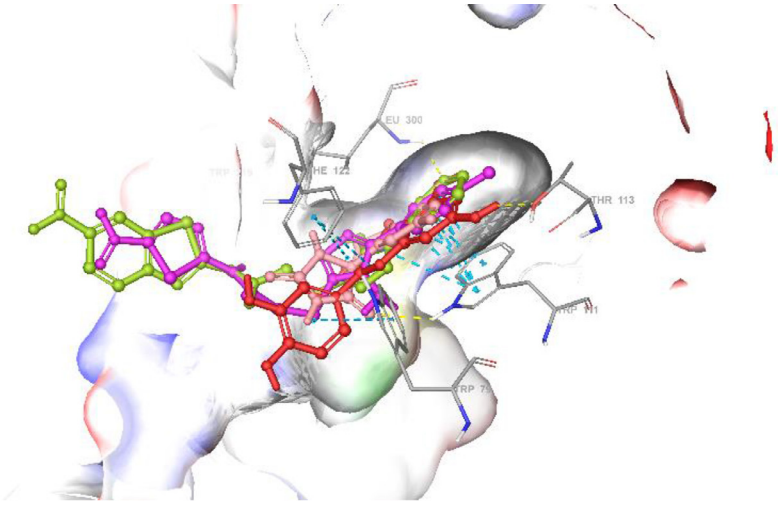

A

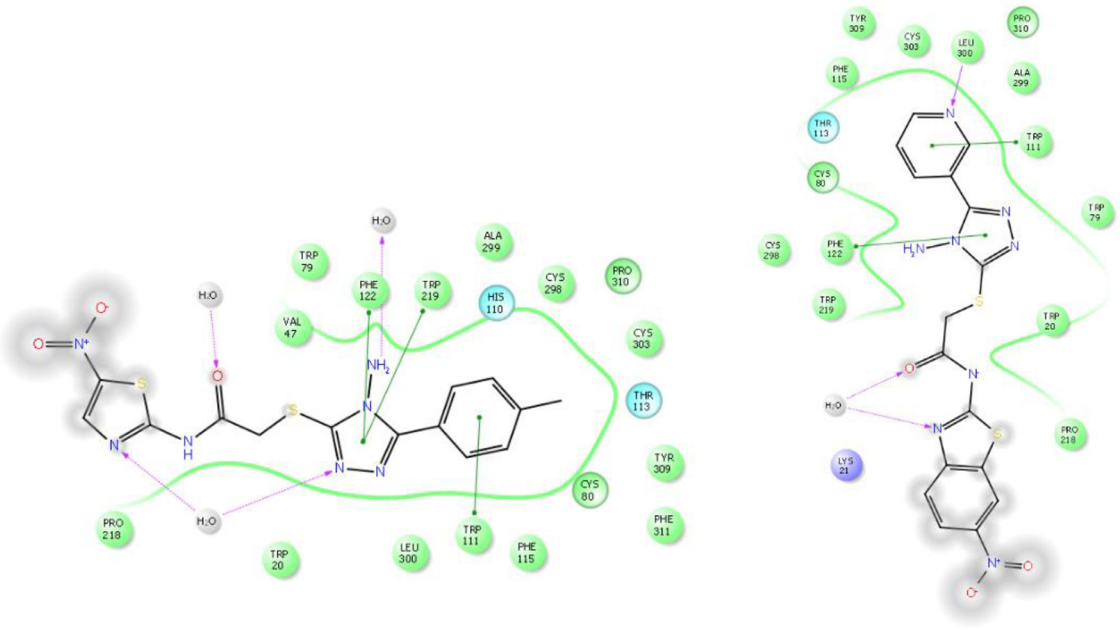

Compound **12** Compound **17**

B

Fig. 6. Docking poses of compounds **12** and **17**, quercetin and sorbinil (**A**) (coloured in purple, yellow green, red and pink, respectively) and docking interactions of compounds **12** and **17** (**B**) in the active site of AR (Blue and green dashes: π-π interactions, yellow dashes: hydrogen bonding).

Table 2
The IC_{50}, K_i values and inhibition types for compounds **1**–**18**.

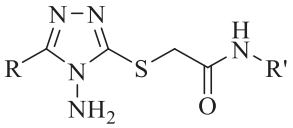

Compound	R	R'	IC_{50} (μM)	R^2	K_i (μM)	Type of Inhibition
1	4-Methoxyphenyl	Benzothiazol-2-yl	0.213	0.9857	0.33 ± 0.08	Non-Competitive
2	4-Methoxyphenyl	6-Chlorobenzothiazol-2-yl	0.205	0.9812	0.41 ± 0.02	Non-Competitive
3	4-Methoxyphenyl	6-Bromobenzothiazol-2-yl	0.226	0.9820	0.19 ± 0.01	Competitive
4	4-Methoxyphenyl	6-Methylbenzothiazol-2-yl	0.232	0.9814	0.47 ± 0.06	Non-Competitive
5	4-Methoxyphenyl	6-Nitrobenzothiazol-2-yl	0.273	0.9903	0.40 ± 0.03	Non-Competitive
6	4-Methoxyphenyl	5-Nitrothiazole-2-yl	0.291	0.9781	0.50 ± 0.14	Competitive
7	4-Methylphenyl	Benzothiazol-2-yl	0.256	0.9733	0.45 ± 0.02	Non-Competitive
8	4-Methylphenyl	6-Chlorobenzothiazol-2-yl	0.330	0.9747	0.58 ± 0.06	Non-Competitive
9	4-Methylphenyl	6-Bromobenzothiazol-2-yl	0.307	0.9888	0.54 ± 0.06	Non-Competitive
10	4-Methylphenyl	6-Methylbenzothiazol-2-yl	0.346	0.9836	0.81 ± 0.11	Non-Competitive
11	4-Methylphenyl	6-Nitrobenzothiazol-2-yl	0.243	0.9833	0.42 ± 0.05	Non-Competitive
12	4-Methylphenyl	5-Nitrothiazole-2-yl	0.294	0.9874	0.04 ± 0.01	Competitive
13	Pyridin-3-yl	Benzothiazol-2-yl	0.260	0.9768	0.61 ± 0.02	Non-Competitive
14	Pyridin-3-yl	6-Chlorobenzothiazol-2-yl	0.302	0.9760	0.28 ± 0.09	Competitive
15	Pyridin-3-yl	6-Bromobenzothiazol-2-yl	0.308	0.9836	0.32 ± 0.08	Competitive
16	Pyridin-3-yl	6-Methylbenzothiazol-2-yl	0.257	0.9863	0.25 ± 0.07	Non-Competitive
17	Pyridin-3-yl	6-Nitrobenzothiazol-2-yl	0.311	0.9737	0.08 ± 0.02	Competitive
18	Pyridin-3-yl	5-Nitrothiazole-2-yl	0.232	0.9825	0.23 ± 0.03	Non-Competitive
Quarcetin	–	–	3.860	0.9837	5.66 ± 0.66	Non-Competitive

Table 5
Predicted ADME properties of compounds **1**–**18**.

Compound	CIQPlogS[a] (−6.5 to 0.5)	QPlogBB[a] (−3 to 1.2)	QPlogKhsa[a] (−1.5 to 1.5)	QPlogPo/w[a] (−2.0 to 6.5)	Rule of Five	Rule of Three
1	−4.208	−1.088	−0.063	2.006	0	0
2	−4.870	−0.949	0.034	2.480	0	0
3	−5.739	−0.943	0.054	2.553	0	0
4	−4.476	−1.136	0.070	2.290	0	0
5	−4.704	−2.304	−0.107	1.312	1	1
6	−3.513	−2.251	−0.415	0.339	1	1
7	−4.172	−1.014	0.063	2.216	1	1
8	−4.835	−0.874	0.169	2.693	0	0
9	−5.705	−0.868	0.183	2.766	0	0
10	−4.441	−1.060	0.200	2.503	0	0
11	−4.673	−2.236	0.023	1.527	0	1
12	−3.481	−2.205	−0.290	0.524	0	1
13	−3.395	−1.283	−0.330	1.042	0	0
14	−4.040	−1.150	−0.239	1.509	0	0
15	−4.891	−1.146	−0.221	1.581	0	0
16	−3.656	−1.314	−0.207	1.336	0	0
17	−3.876	−2.459	−0.380	0.362	1	1
18	−2.711	−2.403	−0.663	−0.606	1	1

[a] CIQPlogS: Conformation-independent predicted aqueous solubility, log S. S in mol dm^{-3} is the concentration of the solute in a saturated solution that is in equilibrium with the crystalline solid, QPlogBB: brain/blood partition coefficient, QPlogKhsa: Prediction of binding to human serum albumin, QPlogPo/w: Predicted octanol/water partition coefficient.

like molecules have octanol/water partition coefficient (QPlogPo/w) < 5, molecular weight < 500, number of hydrogen bond acceptors ≤ 10, and number of hydrogen bond donors ≤ 5. Based on Lipinski's rule, these compounds can be considered as drug-like molecules. On the other hand, the three rules of Jorgensen's rule are aqueous solubility (QPlogS) > −5.7, apparent Caco-2 cell permeability (QPPCaco in nm/s) > 22 nm/s, # primary metabolites < 7. Compounds with fewer (and preferably no) violations of these rules are more likely to be orally bioavailable agents. On the basis of these findings, all compounds are expected to have good oral bioavailability.

4. Conclusion

In this study, new 4*H*-1,2,4-triazole derivatives carrying thiazole/benzothiazole scaffolds (**1**–**18**) were synthesized *via* the nucleophilic substitution reaction of 2–chloro–*N*-(thiazol/benzothiazol-2-yl)acetamides with 4-amino-5-aryl-*4H*-1,2,4-triazole-3-thiol (**A**), which was obtained *via* the reaction of 5-aryl-1,3,4-oxadiazole-2-thiol with hydrazine hydrate. The structures of all compounds were confirmed by IR, ^{1}H NMR, ^{13}C NMR and HRMS data. Compounds **1**–**18** were investigated for their inhibitory effects on AR, which was known as a substantial target in the treatment of some diabetes-linked abnormalities such as cataract, retinopathy, nephropathy and neuropathy. According to *in vitro* studies, compounds **1**–**18** inhibited AR more notably than quercetin. Among them, compounds **12** and **17** were the most pronounced competitive AR inhibitors with the K_i values of 0.04±0.01 μM and 0.08±0.02 μM, respectively. Cytotoxicity studies place a great emphasis on the design and development of new AR inhibitors. The results of MTT assay indicated that apart from compounds **10, 13, 14, 15** and **16**, compounds **1**–**18** were found nontoxic against L929 mouse fibrob-

last (healthy) cells. Molecular docking studies confirmed that compounds **1**–**18**, apart from compound **10**, forged fundamental interactions with Trp219, Phe122 and Trp111 in the active site of AR. According to *in silico* ADME studies, compounds **1**–**18** were expected to possess conceivable pharmacokinetic profiles. Overall, compounds **1**–**18**, excluding compounds **10, 13, 14, 15** and **16**, draw attention as outstanding AR inhibitors for further investigations about diabetic complications.

Declaration of Competing Interest

The authors declare that they have no known competing financial interests or personal relationships that could have appeared to influence the work reported in this paper.

CRediT authorship contribution statement

Belgin Sever: Conceptualization, Data curation, Formal analysis, Funding acquisition, Investigation, Methodology, Project administration, Resources, Software, Supervision, Validation, Visualization, Writing - original draft, Writing - review & editing. **Mehlika Dilek Altıntop:** Conceptualization, Funding acquisition, Methodology, Project administration, Resources, Software, Supervision, Writing - review & editing. **Yeliz Demir:** Data curation, Formal analysis, Methodology, Resources, Software, Validation, Writing - review & editing. **Muhammed Pekdoğan:** Methodology, Software, Writing - review & editing. **Gülşen Akalın Çiftçi:** Data curation, Formal analysis, Methodology, Resources, Software, Validation, Writing - review & editing. **Şükrü Beydemir:** Conceptualization, Methodology, Resources, Supervision, Writing - review & editing. **Ahmet Özdemir:** Conceptualization, Resources, Supervision, Writing - review & editing.

Acknowledgements

This study was supported by Anadolu University Scientific Research Project Commission under the grant no: 2005S026 and Ardahan University Scientific Research Projects Commission under the grant no: 2019–008.

Supplementary materials

Supplementary material associated with this article can be found, in the online version, at doi:10.1016/j.molstruc.2020.129446.

References

[1] A. Artasensi, A. Pedretti, G. Vistoli, L. Fumagalli, Type 2 diabetes mellitus: a review of multi-target drugs, Molecules 163 (2010) 51–59.
[2] P. Taslimi, F.M. Kandemir, Y. Demir, M. İleritürk, Y. Temel, C. Caglayan, İ. Gulçin, The antidiabetic and anticholinergic effects of chrysin on cyclophosphamide-induced multiple organ toxicity in rats: pharmacological evaluation of some metabolic enzyme activities, J. Biochem. Mol. Toxicol. 33 (2019) e22313P.
[3] Y. Demir, P. Taslimi, M.S. Ozaslan, N. Oztaskin, Y. Çetinkaya, İ. Gulçin, Ş. Beydemir, S. Goksu, Antidiabetic potential: *in vitro* inhibition effects of bromophenol and diarylmethanones derivatives on metabolic enzymes, Arch. Pharm. (Weinheim) 351 (2018) e1800263.
[4] L. Costantino, G. Rastelli, P. Vianello, G. Cignarella, D. Barlocco, Diabetes complications and their potential prevention: aldose reductase inhibition and other approaches, Med. Res. Rev. 19 (1999) 3–23.
[5] P. Zimmet, K.G. Alberti, J. Shaw, Global and societal implications of the diabetes epidemic, Nature 414 (2001) 782–787.
[6] F. Erdemir, D.B. Celepci, A. Aktaş, Y. Gök, R. Kaya, P. Taslimi, Y. Demir, İ. Gulçin, Novel 2-aminopyridine liganded Pd(II) *N*-heterocyclic carbene complexes: synthesis, characterization, crystal structure and bioactivity properties, Bioorg. Chem. 91 (2019) 103134.
[7] C. Türkeş, Y. Demir, Ş. Beydemir, Anti-diabetic properties of calcium channel blockers: inhibition effects on aldose reductase enzyme activity, Appl. Biochem. Biotechnol. 189 (2019) 318–329.
[8] S.S. Chung, S.K. Chung, Aldose reductase in diabetic microvascular complications, Curr. Drug Targets 6 (2005) 475–486.
[9] A.S. Grewal, S. Bhardwaj, D. Pandita, V. Lather, B.S. Sekhon, Updates on aldose reductase inhibitors for management of diabetic complications and non-diabetic diseases, Mini Rev. Med. Chem. 16 (2016) 120–162.
[10] D.R. Tomlinson, E.J. Stevens, L.T. Diemel, Aldose reductase inhibitors and their potential for the treatment of diabetic complications, Trends Pharmacol. Sci. 15 (1994) 293–297.
[11] C. Caglayan, Y. Demir, S. Kucukler, P. Taslimi, F.M. Kandemir, İ. Gulçin, The effects of hesperidin on sodium arsenite-induced different organ toxicity in rats on metabolic enzymes as antidiabetic and anticholinergics potentials: a biochemical approach, J. Food Biochem. 43 (2019) e12720.
[12] C. Çağlayan, P. Taslimi, Y. Demir, S. Küçükler, F.M. Kandemir, İ. Gulçin, The effects of zingerone against vancomycin-induced lung, liver, kidney and testis toxicity in rats: the behavior of some metabolic enzymes, J. Biochem. Mol. Toxicol. 33 (2019) e22381.
[13] Y. Demir, H.E. Duran, L. Durmaz, P. Taslimi, Ş. Beydemir, İ. Gulçin, The influence of some nonsteroidal anti-inflammatory drugs on metabolic enzymes of aldose reductase, sorbitol dehydrogenase, and α-glycosidase: a perspective for metabolic disorders, Appl. Biochem. Biotechnol. 190 (2020) 437–447.
[14] Y. Demir, M.S. Özaslan, H.E. Duran, Ö.İ. Küfrevioğlu, Ş. Beydemir, Inhibition effects of quinones on aldose reductase: antidiabetic properties, Environ. Toxicol. Pharmacol. 70 (2019) 103195.
[15] Y. Demir, Z. Köksal, Some sulfonamides as aldose reductase inhibitors: therapeutic approach in diabetes, Arch. Physiol. Biochem. (2020), doi:10.1080/13813455.2020.1742166.
[16] R. Ramasamy, S.F. Yan, A.M. Schmidt, Polyol pathway and RAGE: a central metabolic and signaling axis in diabetic complications, Expert Rev. Endocrinol. Metab. 5 (2010) 65–75.
[17] A.M. Warren, S.T. Knudsen, M.E. Cooper, Diabetic nephropathy: an insight into molecular mechanisms and emerging therapies, Expert Opin. Ther. Targets 23 (2019) 579–591.
[18] J.M. Petrash, All in the family: aldose reductase and closely related aldo-keto reductases, Cell. Mol. Life Sci. 61 (2004) 737–749.
[19] K.V. Ramana, S.K. Srivastava, Aldose reductase: a novel therapeutic target for inflammatory pathologies, Int. J. Biochem. Cell Biol. 42 (2010) 17–20.
[20] P.J. Oates, B.L. Mylari, Aldose reductase inhibitors: therapeutic implications for diabetic complications, Expert Opin. Investig. Drugs 8 (1999) 2095–2119.
[21] S. Miyamoto, Recent advances in aldose reductase inhibitors: potential agents for the treatment of diabetic complications, Expert Opin. Ther. Pat. 12 (2002) 621–631.
[22] R. Maccari, R. Ottanà, Targeting aldose reductase for the treatment of diabetes complications and inflammatory diseases: new insights and future directions, J. Med. Chem. 58 (2015) 2047–2067.
[23] J. Dowarah, V.P. Singh, Anti-Diabetic drugs recent approaches and advancements, Bioorg. Med. Chem. 28 (2020) 115263.
[24] S.B. Ferreira, A.C. Sodero, M.F. Cardoso, E.S. Lima, C.R. Kaiser, F.P. Silva, V.F. Ferreira, Synthesis, biological activity, and molecular modeling studies of 1*H*-1,2,3-triazole derivatives of carbohydrates as α-glucosidases inhibitors, J. Med. Chem. 53 (2010) 2364–2375.
[25] R. Kharb, P.C. Sharma, M.S. Yar, Pharmacological significance of triazole scaffold, J. Enzyme Inhib. Med. Chem. 26 (2011) 1–21.
[26] L. Guo, D.L. Parker, Y. Zang, R.F. Sweis, W. Liu, E.C. Sherer, N. Buist, J. Terebetski, T. Kelly, R. Bugianesi, B.T. Priest, K.H. Dingley, X. Li, S. Mitelman, G. Salituro, M.E. Trujillo, M. Pachanski, M. Kirkland, M.A. Powles, G.J. Eiermann, Y. Feng, J. Shang, A.D. Howard, F. Ujjainwalla, C.J. Sinz, J.S. Debenham, S.D. Edmondson, R.P. Nargund, W.K. Hagmann, D. Li, Discovery and optimization of a novel triazole series of GPR142 agonists for the treatment of type 2 diabetes, ACS Med. Chem. Lett. 7 (2016) 1107–1111.
[27] B. Sever, M.D. Altıntop, G. Kuş, M. Özkurt, A. Özdemir, Z.A. Kaplancıklı, Indomethacin based new triazolothiadiazine derivatives: synthesis, evaluation of their anticancer effects on T98 human glioma cell line related to COX-2 inhibition and docking studies, Eur. J. Med. Chem. 113 (2016) 179–186.
[28] D. Dheer, V. Singh, R. Shankar, Medicinal attributes of 1,2,3-triazoles: current developments, Bioorg. Chem. 71 (2017) 30–54.
[29] G. Wang, Z. Peng, J. Wang, X. Li, J. Li, Synthesis, *in vitro* evaluation and molecular docking studies of novel triazine-triazole derivatives as potential α-glucosidase inhibitors, Eur. J. Med. Chem. 125 (2017) 423–429.
[30] S. Zhang, Z. Xu, C. Gao, Q.C. Ren, L. Chang, Z.S. Lv, L.S. Feng, Triazole derivatives and their anti-tubercular activity, Eur. J. Med. Chem. 138 (2017) 501–513.
[31] E. Kyriakis, T.G.A. Solovou, S. Kun, K. Czifrák, B. Szőcs, L. Juhász, É. Bokor, G.A. Stravodimos, A.L. Kantsadi, D.S.M. Chatzileontiadou, V.T. Skamnaki, L. Somsák, D.D. Leonidas, Probing the β;-pocket of the active site of human liver glycogen phosphorylase with 3-(c-β;-D-glucopyranosyl)-5-(4-substituted-phenyl)-1,2,4-triazole inhibitors, Bioorg. Chem. 77 (2018) 485–493.
[32] K. Bozorov, J. Zhao, H.A. Aisa, 1,2,3-Triazole-containing hybrids as leads in medicinal chemistry: a recent overview, Bioorg. Med. Chem. 27 (2019) 3511–3531.
[33] N.K. Verma, D. Mondal, S. Bera, Pharmacological and cellular significance of triazole-surrogated compounds, Curr. Org. Chem. 23 (2019) 2505–2572.
[34] Kanwal E.O.Yeye, K.M. Khan, S. Chigurupati, A. Wadood, A.U. Rehman, S. Perveen, M.K. Maharajan, S. Shamim, S. Hameed, S.A. Aboaba, M. Taha, Syntheses, *in vitro* α-amylase and α-glucosidase dual inhibitory activities of 4-amino-1,2,4-triazole derivatives their molecular docking and kinetic studies, Bioorg. Med. Chem. 28 (2020) 115467.
[35] A. Ibrar, Y. Tehseen, I. Khan, A. Hameed, A. Saeed, N. Furtmann, J. Bajorath, J. Iqbal, Coumarin-thiazole and -oxadiazole derivatives: synthesis, bioactivity

and docking studies for aldose/aldehyde reductase inhibitors, Bioorg. Chem. 68 (2016) 177–186.
[36] G.L. Khatik, A.K. Datusalia, W. Ahsan, P. Kaur, M. Vyas, A. Mittal, S.K. Nayak, A retrospect study on thiazole derivatives as the potential antidiabetic agents in drug discovery and developments, Curr. Drug Discov. Technol. 15 (2018) 163–177.
[37] B. Sever, M.D. Altıntop, Y. Demir, G. Akalın Çiftçi, Ş. Beydemir, A. Özdemir, Design, synthesis, *in vitro* and *in silico* investigation of aldose reductase inhibitory effects of new thiazole-based compounds, Bioorg. Chem. 102 (2020) 104110.
[38] T.N.V. Ganesh Kumar, G. Gautham Shenoy, S.S. Kar, V. Shenoy, I. Bairy, Design, synthesis and evaluation of antitubercular activity of novel 1,2,4-triazoles against MDR strain of *Mycobacterium tuberculosis*, Pharm. Chem. J. 51 (2018) 907–917.
[39] M.D. Altıntop, Z.A. Kaplancikli, G. Turan-Zitouni, A. Özdemir, F. Demirci, G. Iscan, G. Revial, Synthesis of some novel triazole derivatives and investigation of their antimicrobial activities, Synthetic Commun 41 (2011) 2234–2250.
[40] M.D. Altıntop, B. Sever, G. Akalın Çiftçi, G. Turan-Zitouni, Z.A. Kaplancıklı, A. Özdemir, Design, synthesis, *in vitro* and *in silico* evaluation of a new series of oxadiazole-based anticancer agents as potential Akt and FAK inhibitors, Eur. J. Med. Chem. 155 (2018) 905–924.
[41] M.J. Cerelli, D.L. Curtis, J.P. Dunn, P.H. Nelson, T.M. Peak, L.D. Waterbury, Antiinflammatory and aldose reductase inhibitory activity of some tricyclic arylacetic acids, J. Med. Chem. 29 (1986) 2347–2351.
[42] Y. Demir, M. Işık, I. Gülçin, Ş. Beydemir, Phenolic compounds inhibit the aldose reductase enzyme from the sheep kidney, J. Biochem. Mol. Toxicol. 31 (2017) e21936.
[43] M.M. Bradford, A rapid and sensitive method for the quantitation of microgram quantities of protein utilizing the principle of protein-dye binding, Anal. Biochem. 72 (1976) 248–254.
[44] U.K. Laemmli, Cleavage of structural proteins during the assembly of the head of bacteriophage T4, Nature 227 (1970) 680–685.
[45] Y. Demir, Naphthoquinones, benzoquinones, and anthraquinones: molecular docking, ADME and inhibition studies on human serum paraoxonase-1 associated with cardiovascular diseases, Drug Dev. Res 81 (2020) 628–636.
[46] Y. Demir, C. Türkeş, Ş. Beydemir, Molecular docking studies and ınhibition properties of some antineoplastic agents against paraoxonase-I, Anticancer Agents Med. Chem. 20 (2020) 887–896.
[47] Y. Demir, The behaviour of some antihypertension drugs on human serum paraoxonase-1: an important protector enzyme against atherosclerosis, J. Pharm. Pharmacol. 71 (2019) 1576–1583.
[48] M. Işık, Ş. Beydemir, Y. Demir, M. Durgun, C. Türkeş, A. Nasır, A. Necip, M. Akkuş, Benzenesulfonamide derivatives containing imine and amine groups: inhibition on human paraoxonase and molecular docking studies, Int. J. Biol. Macromol. 146 (2020) 1111–1123.
[49] Q. Istrefi, C. Türkeş, M. Arslan, Y. Demir, A.R. Nixha, Ş. Beydemir, Ö.İ. Küfrevioğlu, Sulfonamides incorporating ketene *N,S*-acetal bioisosteres as potent carbonic anhydrase and acetylcholinesterase inhibitors, Arch. Pharm. (Weinheim) 353 (2020) 1900383.
[50] M. Işık, Y. Demir, M. Durgun, C. Türkeş, A. Necip, Ş. Beydemir, Molecular docking and investigation of 4-(benzylideneamino)- and 4-(benzylamino)-benzenesulfonamide derivatives as potent AChE inhibitors, Chem. Pap. 74 (2020) 1395–1405.
[51] H. Lineweaver, D. Burk, The determination of enzyme dissociation constants, J. Am. Chem. Soc. 56 (1934) 658–666.
[52] M. Durgun, C. Türkeş, M. Işık, Y. Demir, A. Saklı, A. Kuru, A. Güzel, Ş. Beydemir, S. Akocak, S.M. Osman, Z. AlOthman, C.T. Supuran, Synthesis, characterisation, biological evaluation and *in silico* studies of sulphonamide schiff bases, J. Enzyme Inhib. Med. Chem. 35 (2020) 950–962.
[53] C. Türkeş, Investigation of potential paraoxonase-I inhibitors by kinetic and molecular docking studies: chemotherapeutic drugs, Protein Pept. Lett. 26 (2019) 392–402.
[54] C. Türkeş, Y. Demir, Ş. Beydemir, Calcium channel blockers: molecular docking and inhibition studies on carbonic anhydrase I and II isoenzymes, J. Biomol. Struct. Dyn. (2020), doi:10.1080/07391102.2020.1736631.
[55] T. Mosmann, Rapid colorimetric assay for cellular growth and survival: application to proliferation and cytotoxicity assays, J. Immunol. Methods. 16 (1983) 55–63.
[56] F. Ruiz, I. Hazemann, A. Mitschler, A. Joachimiak, T. Schneider, M. Karplus, A. Podjarny, The crystallographic structure of the aldose reductase-IDD552 complex shows direct proton donation from tyrosine 48, Acta Crystallogr. D Biol. Crystallogr. 60 (2004) 1347–1354.
[57] Z. Alim, N. Kilinç, B. Şengül, Ş. Beydemir, Inhibition behaviours of some phenolic acids on rat kidney aldose reductase enzyme: an *in vitro* study, J. Enzyme Inhib. Med. Chem. 32 (2017) 277–284.
[58] H.E. Aslan, Ş. Beydemir, Phenolic compounds: the inhibition effect on polyol pathway enzymes, Chem. Biol. Interact. 266 (2017) 47–55.
[59] P. Taslimi, H.E. Aslan, Y. Demir, N. Öztaşkın, A. Maraş, İ. Gülçin, Ş. Beydemir, S. Göksu, Diarylmethanon, bromophenol and diarylmethane compounds: discovery of potent aldose reductase, α-amylase and α-glycosidase inhibitors as new therapeutic approach in diabetes and functional hyperglycemia, Int. J. Biol. Macromol. 119 (2018) 857–863.
[60] F. Da Settimo, G. Primofiore, A. Da Settimo, C. La Motta, F. Simorini, E. Novellino, G. Greco, A. Lavecchia, E. Boldrini, Novel, highly potent aldose reductase inhibitors: cyano(2-oxo-2,3-dihydroindol-3-yl)acetic acid derivatives, J. Med. Chem. 46 (2003) 1419–1428.
[61] T.H. Kim, J.K. Kim, Y.H. Kang, J.Y. Lee, I.J. Kang, S.S. Lim, Aldose reductase inhibitory activity of compounds from *Zea mays* L., Biomed. Res. Int. (2013) (2013) 727143.
[62] B.T. Burlingham, T.S. Widlanski, An intuitive look at the relationship of K_i and IC_{50}: a more general use for the dixon plot, J. Chem. Educ. 80 (2003) 214–218.
[63] P. Alexiou, K. Pegklidou, M. Chatzopoulou, I. Nicolaou, V.J. Demopoulos, Aldose reductase enzyme and its implication to major health problems of the 21st century, Curr. Med. Chem. 16 (2009) 734–752.
[64] J.N. Sangshetti, R.S. Chouthe, N.S. Sakle, I. Gonjari, D.B. Shinde, Aldose reductase: a multi-disease target, Curr. Enzym. Inhib. 10 (2014) 2–12.
[65] G. Van Den Driessche, D. Fourches, Adverse drug reactions triggered by the common HLA-B*57:01 variant: a molecular docking study, J. Cheminform. 9 (2017) 13.